CEEGS DELIVERABLE D2.2

Assessment of the impact of geological conditions on the efficiency of the system

Summary:

Numerical and semi-analytical simulations are conducted to understand how the transient behaviour of P and T in boreholes and geological reservoirs during the charge/discharge cycles affect the overall efficiency of the system. Tested geological scenarios include Deep Saline Aquifers, Geothermal reservoirs, and Salt dissolution cavities, in multiple configurations. The porous media scenarios (wellbores and reservoirs) are modelled numerically using the software CMG and the impact of the geological conditions to the CEEGS feasibility is assessed through well indexes, such as injectivity and productivity, and through gross efficiency, while a sensitivity analysis defines the relative importance of different reservoir parameters. The salt cavities scenarios are studied using a semi-analytical approach that integrates salt cavity, wellbores and surface facilities to obtain the efficiency of the system for different cavity depths.

Authors:

Dounya Behnous[1], Márton Farkas[2], Andrés Carro[3], Ricardo Chacartegui[3], Júlio Carneiro[1]

[1]Converge!, Lda; [2]GFZ Potsdam; [3]University of Seville

Funded by the European Union

Title:	Assessment of the impact of geological conditions on the efficiency of the system
Lead beneficiary:	CONV
Other beneficiaries:	GFZ, USE
Due date:	December 2023
Nature:	Public
Diffusion:	Public
Status:	Live document
DOI:	
License information:	
Recommended Citation:	Behnous, D., Farkas, M., Carro, A., Chacartegui, R. and Carneiro, J. (2023) - Assessment of the impact of geological conditions on the efficiency of the system. Deliverable D2.2 CEEGS. Évora, 40 pp.
Related Data:	
ORCID:	
Document code:	CEEGS_D.2.2

Revision history	Author	Delivery date	Summary of changes and comments
Version 01	JFC	11.12.2023	First version
Version 02	JFC	23.12.2023	Public version
Final version			

Approval status				
	Name	Function	Date	Signature
Deliverable responsible	Júlio Carneiro	Editor	11.12.2023	
WP leader	Júlio Carneiro	WP leader	11.12.2023	
Reviewer				
Reviewer				
Project Coordinator				

Funded by the European Union. Views and opinions expressed are however those of the author(s) only and do not necessarily reflect those of the European Union or CINEA. Neither the European Union nor the granting authority can be held responsible for them.

TABLE OF CONTENTS

FIGURES

TABLES

EXECUTIVE SUMMARY

CEEGS is inherently a technology that operates in cycles of charge and discharge, in which the transient pressure and temperature conditions at the geological reservoir and at the wellbores constrain the feasibility and efficiency of the system. The aim of this report is to clarify how the transient behaviour of P and T in the wellheads and bottomholes during the charge/discharge cycles and the reservoir conditions affect the overall efficiency of the system. The overarching goal is to further constrains the geological reservoir and technology configurations that are most suitable for early implementation of the technology.

Several geological scenarios were studied, including deep saline aquifers (open and closed boundaries conditions), two deep saline aquifers at different depths and geothermal reservoir. Several variants or configurations were studied in some of those scenarios. Additionally, salt cavities were also considered as a potential geological reservoir.

The approach to the porous media reservoirs and salt cavities was different, since porous media are much more complex geological environments than salt cavities, with the former being studied with numerical tools encompassing only the subsurface components, and the latter with semi-analytical solutions that include both subsurface and surface plant components.

To ensure that CEESG was tested under realistic conditions, real-world data was used for the porous media simulations, using information from geological reservoirs being considered for CO_2 storage in Portugal and Spain or that are being used for geothermal energy purposes in Germany. Extensive sensitivity analyses were implemented to understand the relevance of the different geological and engineering parameters.

The simulations favour deeper aquifer or geothermal systems for implementation of CEEGS, with the shallower aquifers (be it a single injection and production aquifer, or two aquifers at different depths) providing lower efficiencies since the CO_2 is produced as a gas. The closed boundaries deep saline aquifer also raised concerns about the amount of brine co-produced with the CO_2, and imposing lower mass flow rates due to pressure buildup limits.

The open boundaries deep saline aquifer scenario, at high reservoir depth, and the geothermal scenario retrieve the most interesting gross efficiencies and sustainability, assessed by the well injectivities and well productivities, reflecting the added contribution of geothermal heat to the temperatures of the produced CO_2.

In the scenarios with salt cavities to store CO_2 in the charge-discharge cycles the round-trip efficiencies was found to range from 47.2% to 55.2 %, for salt cavities ranging in depth from 500 m to 1500 m, but further optimization of the surface components may lead to even higher efficiencies.

Several concerns need to be addressed in subsequent tasks: i) the chemical composition of the fluid at the producing wellhead, due to geochemical reactions between CO_2-rock-brine in the reservoir - to be addressed in task 2.3; ii) the difficulties imposed by the intermittency of injection and production of CO_2 - to be studied in WP3 and WP4; iii) the impacts of heterogeneity and anisotropy to the saturation levels around the production wells, issues that should be addressed when simulating the Ketzin and Hontomin reservoirs.

The main body of this deliverable, from chapter 1 to chapter 4 is of public distribution, while the appendices, given the potential exploitation of Intellectual Property associated with the CEEGS technology, are restricted to the consortium.

1 INTRODUCTION

The efficiency of the open-cycle CEEGS technology, with CO_2 injection in geological formations during the charge stage and CO_2 production during the discharge stage is dependent on the Pressure (P) and Temperature (T) conditions at the reservoir, on the P&T variations between wellheads and bottomholes, and on the kinetics of CO_2 trapping mechanisms in the subsurface. The need to balance the P-T subsurface conditions to those in the surface energy plant and the need to balance CO_2 permanent trapping and maintenance of a CO_2 injection/production cycle implies that the technology efficiency will vary with the geological environment and conditions. The overall objective of WP2 is to identify the geological scenarios in which the CEEGS technology can be most efficient.

Task 2.1 studied the most suitable geological scenarios utilising a semi-analytical approach that focused on the steady state behaviour of the system. However, CEEGS is inherently a technology that operates in cycles and in which the transient P&T imposed by the geological conditions will be of paramount importance to the feasibility and efficiency of the system. That is the aim of task 2.2 and of this report; to understand how the transient behaviour of P and T in the wellheads and bottomholes during the charge/discharge cycles and the influence of the geological setting on the overall efficiency of the system. The overarching goal is to further constrains the geological reservoir and technology configurations that are most suitable for early implementation of the technology.

Given the results in task 2.1 and reported in deliverable D2.1 the geological scenarios addressed in this report are listed in Table 1.

Table 1: Geological scenarios

Geological Environment	Reservoir type
Porous media	Deep Saline Aquifer, Open boundaries
	Deep Saline Aquifer, Closed boundaries
	Two deep saline aquifers
	Geothermal reservoir
Salt cavities	One salt dissolution cavity and surface tank
	Two salt dissolution cavities.

Although CEEGS is primarily a CO_2 utilisation technology, CO_2 injection in geological formations should follow the general guidelines set in the CO_2 Capture and Storage (CCS) Directive, with injection in geological formations saturated in high salinity water, that is, Deep Saline Aquifers (DSA). Deliverable D2.1 recommended the study of yet another reservoir type, *depleted hydrocarbon field*, a geological environment also commonly considered for CCS activities. However, since the main expected difference to the deep saline aquifer cases is related to the chemical composition of the CO_2 stream in the production well, and not on the P and T transient behaviour, such scenario will be studied only in task 2.3.

The approach to the porous media reservoirs and salt cavities is different, since porous media are much more complex geological environments than salt cavities. Thus, the porous media scenarios focus on the behaviour of CO_2 in the reservoir and wellbores and do not attempt a joint simulation with the surface components for energy storage, something that will be conducted in WP3. Thus, the methodology for the porous media scenarios was devised to provide an overview of the efficiency of the underground component of the CEEGS technology. On the contrary, the salt cavities scenarios provide a simplified environment and the methodology incorporates the surface energy storage components.

Another important difference between the two geological environments, but also with the approach in deliverable D2.1, is the utilisation of actual field data and geological structures in the porous media scenarios, while the salt cavity scenarios remain conceptual. Therefore, the porous media scenarios presented in this report refer to geological reservoir in Portugal and Spain that are being considered for CO_2 storage or that are being used for geothermal energy purposes in Germany. The decision of using actual field data ensures that realistic conditions (and geological structures) are adopted. Obviously, this comes at a cost since the diversity of geological conditions that can be studied is lower than if a range of conceptual geological models had been adopted. This shortcoming was minimised by conducting extensive sensitivity analysis in the numerical models.

The need to distinguish between the open boundaries and the closed boundaries DSA scenarios aims at understanding the influence that increased pressure build-up and lower storage efficiencies imposed by the closed boundaries scenario (due to impossibility of brine migration) may represent to the feasibility of CEEGS.

The scenario with two DSAs, at different depths, aims to provide a system configuration that may be adequate when multiple permeable reservoirs are accessible at a specific location and understand if that configuration can be more or less efficient than the single DSA configuration.

The geothermal sedimentary system was included in the scenarios (although not inherently different from the single DSA scenario) because the sensitivity analysis conducted in D2.1 proved that the geothermal gradient plays an important role to the plume setup stage, to the expected wellheads pressures and temperature at the production well, and consequently to the efficiency of the whole energy storage system. It also provides the opportunity for a different, simpler, configuration of the wells in the charge-discharge cycles.

This deliverable is organized as follows: chapter two details the methodology and tools, chapter three presents the scenarios, the numerical models and the results of the simulations in what respects the initial plume setup. Chapter four presents conclusions and recommendations for work to be developed in other work packages.

Three appendices provide details about the scenarios and the results: appendix 1 describes the MATLAB tool implemented to simulate CO_2 flow in the wellbore; appendix 2 addresses the integration of surface and subsurface components in the salt cavity scenario; and appendix 3 presents the results for the charge-discharge cycles, both in terms of sustainability metrics and sensitivity analysis for the porous media scenarios and is composed of four parts (A to D), one for each of the porous media scenarios.

The main body of this deliverable, from chapter one to chapter four, is for public distribution, while the appendices, given the potential exploitation of Intellectual Property associated with the CEEGS technology, are confidential and accessible only to the consortium partners.

2 METHODOLOGY

The geological environments tested require different modelling tools to simulate the scenarios of CEEGS implementation: while for porous media reservoirs the diversity of geological parameters and conditions demand the utilization of **numerical modelling tools** (CMG STARS and CMG GEM), the scenarios in salt cavity environments are less prone to involve large geological complexity and were modelled by **semi-analytical tools** (MATLAB and python). Moreover, the wellbore-cavity arrangements in the salt cavity scenarios, being less complex than the porous media scenarios, allow for an integration with the surface components of the CEEGS, providing a more robust analysis of the influence of the underground component to the overall efficiency of the system. This integration of underground and surface components was not attempted for the porous media scenarios and is addressed in WP3.

2.1 NUMERICAL MODELLING TOOLS

CO_2 injection and subsequent CO_2 plume migration in the "Geothermal scenario" and the "Two DSAs scenario" are modelled using **CMG-GEM** commercial subsurface flow simulator, while for the "Closed DSA" and "Open DSA" scenarios the **CMG-STARS** commercial simulator was used (CMG, 2023). CMG-GEM and CMG-STARS are Equation of state (EoS) subsurface simulators for compositional, chemical and hydrodynamical processes that employ the finite volume method to simulate multiphase flow and heat transfer within porous media. The selection of the different CMG simulators was decided based on the different approaches of CMG-GEM and CMG-STARS to the wellbore modelling features, because simulation of pressure and temperature conditions within the CO_2 injection and back-producing wellbores is fundamental to understand the CEEGS efficiency (see deliverable D2.1). The following section describes the approaches used.

2.1.1 Wellbore modelling features

Precise computation of heat transfer between the fluid inside the wellbore and the surrounding formation is crucial. A standard wellbore configuration, illustrated in Figure 1, typically comprises tubing, casing, and cement. When CO_2 flows through the tubing in the wellbore, it undergoes continuous heat exchange with the surrounding formation. During this process, heat can either be gained or lost. Heat transfer mechanisms involved include conduction, forced convection, and natural convection.

CMG-STARS simulator includes the capability to model the wellbore. It calculates the pressure drop along the wellbore and the radial heat loss for both injector and producer wells. This calculation is done semi-analytically using a wellbore model known as the SAM model, which is coupled to the reservoir model. The transfer of heat between the well and the surrounding formation occurs radially through conduction, utilizing a model described by Fontanilla and Aziz in 1982. Both momentum and energy equations are simultaneously solved to assess changes in pressure and enthalpy along the wellbore. The pressure drop is contingent on factors such as friction, gravity, and kinetic energy. The SAM model is intricately linked to the simulator, except for the formation temperature. The temperature gradient between T_{hole} and T_e (as shown in Figure 1 below) is computed within the wellbore model, considering radial heat loss.

The overall heat transfer coefficient is determined from the input data and is contingent on resistivity in the fluid film, tubing wall, insulation, annular space, casing wall, and cement. It is important to note that radial heat loss diminishes over time due to the progressive increase in the surrounding formation temperature. In our simulations, method known as "Regime" is employed. This method is utilized to

compute friction pressure drop and gravity effects, which are contingent upon correlations that are reliant on the flow regime and the type of fluid, be it two-phase or homogeneous. These correlations are primarily based on the work of Xiao et al. (1990).

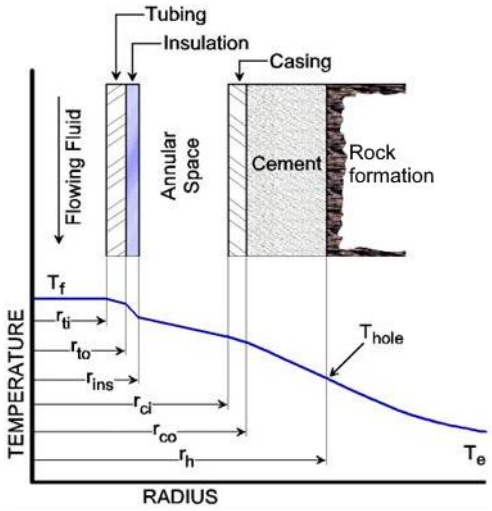

Figure 1: Schematic representation of wellbore model in CMG-STARS (CMG, 2023). Refer to the CMG (2003) manual for definition of different radial distances.

The CMG-GEM reservoir simulator does not come with a built-in wellbore model. Therefore, we have developed a MATLAB code utilizing a semi-analytical model and the CoolProp-MATLAB wrapper (Bell et al., 2014) for the CO_2 properties. The code can simulate pressure and temperature between wellbore wellhead and bottomhole due to CO_2 injection and production. Appendix 1 describes in detail the semi-analytical approach.

2.1.2 Plume setup and well configuration

The subsurface component of CEEGS comprises two main stages. Initially, there is the CO_2 plume setup phase, during which CO_2 is continuously injected for a duration of two years. A substantial quantity of CO_2 is introduced into the reservoirs to ensure the formation of a supercritical CO_2 plume. The energy storage component of CEEGS is inactive during this stage. The presence of the CO_2 plume leads to the lateral displacement of formation water away from the injection wells, reducing the risk of water production during subsequent stages. Additionally, this stage enables CO_2 sequestration through trapping mechanisms within the aquifer.

The second stage involves energy storage with charge-discharge cycles. In the charge phase, surplus renewable electricity is utilized to compress (and heat) and inject CO_2 into the geological reservoir through injection Well A. During the discharge phase, Well A produces supercritical CO_2, which is used in the surface components of CEEGS to produce electricity, after which Well B injects CO_2 in the reservoir at a lower temperature, but same flow rate as Well A.

The initial plume setup is expected to play an important role in the economic feasibility of the system, but also on the relative importance of the components of CO_2 permanent sequestration, energy storage and geothermal heat mining. Task 3.1 will address in detail the strategies and options for setting up a sufficiently large CO_2 plume in the geological reservoir previously to the start of the CEEGS

charge and discharge cycles. Since this report concerns mostly the influence of the geological scenarios on the charge-discharge cycles, the initial CO2 plume setup is less relevant and was simplified.

A two-year CO_2 setup stage was designed with a constant injection rate of 33 kg/s to attain a high level of CO_2 saturation around the bottomhole of the back-producing well. The injection temperature at the outset was set at 20°C, with the CO_2 being provided directly from a CO2 capture facility.

During the charge and discharge phases, Well A injects CO_2 at a wellhead temperature of 60°C, while Well B remains inactive. In the discharge phase, Well A produces CO_2, which is later injected, at the same flow rate, through Well B at a temperature of 20°C. It is important to note that the injection wells have two constraints, the first is the bottomhole pressure constraint, requiring the pressure buildup to remain below 20% of the initial hydrostatic pressure. The second is the injection pressure needed to convey the CO_2 to the bottom of the reservoir. The cycles of charge-shut in-discharge was repeated six times.

Depending on geological scenario, a single well or two wells were considered for the charge-discharge cycles. More complex well configurations will be studied in WP4 of the CEEGS project. For the sake of simplicity, only vertical wells are considered. Specific arrangements of wells vary between scenarios and are described in the appendices.

2.1.3 Charge / discharge cycles

After plume setup, the injection well is shut in for a period of 30 days to allow recovery, after which the energy storage cycle starts. In every case, a uniform, 24-hour-long energy storage cycle is developed that consists of four phases after the CO_2 plume is established:

1. Discharge phase for 6 hours;
2. Shut-in or recovery period during which the injection and production wells are shut-in for 6 hours;
3. Charge phase for 6 hours; and
4. Shut-in or recovery period for 6 hours.

After the shut-in phase, the storage cycle is repeated five more times, starting with another discharge period. The duration of each phase is controlled by supply and demand; thus, they are prone to daily variation. In this deliverable, we propose a simplified energy storage cycle with equally distributed durations. This scheme addresses the need for intra-day energy buffer capacity.

Later in WP3, on a similar basis, long-term or seasonal energy storage cycle will be considered where excess energy generated in one season is stored for use in another season. In this case, each phase could last for 3 months.

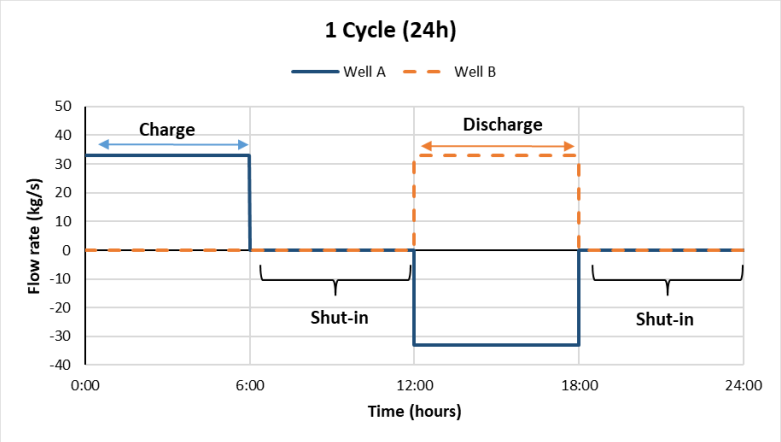

Figure 2: Schematic representation of the charge-discharge cycles and operating mode of wells. Some differences exist in the geothermal scenario and will be described in detail in the relevant section.

2.2 SEMI-ANALYTICAL MODEL FOR SALT CAVITIES SCENARIOS

The scenarios considering salt cavities to store CO_2 are implemented following the methodology and assumptions indicated in deliverable D2.1. Experimental investigations on rock salt cores subjected to supercritical CO_2 pressurization showed that a pressure-driven opening of grain boundaries occurs in polycrystalline rock salt and thus a loss of tightness only occurs when the CO_2 pressure significantly exceeds the minimum principal stress (Minkley et al. 2022). This means that the maximum storage pressure is limited by the minimum principal stress in the salt rock acting on the cavern roof, i.e., by the lithostatic pressure (Soubeyran et al., 2019). Therefore, the allowable pressures in salt caverns are considerably higher than those allowable in porous media (often restricted to 20% of the initial hydrostatic pressure).

Following the maximum and minimum pressure values used as pressure limits in the CAES industry and defined by Allen et al. (1982) (and followed by Soubeyran et al. (2019)) as:

$$P_{min}^{\text{salt,cavs}} = \max\left(0.3 * P_{lith}^{\text{salt,cavs}}; \mathrm{P}_{CO2}^{Crit}\right)$$

$$P_{max}^{\text{salt,cavs}} = 0.8 * P_{lith}^{\text{salt,cavs}}$$

This minimum pressure is necessary to avoid cavity closure and is maintained by the cushion gas and is kept above the critical pressure to ensure the supercritical behaviour of the CO_2 in the plume. To ensure supercritical CO_2 behaviour, considering different pressure and temperature gradients and operating the cavity close to the minimum pressure imposed by the cushion gas, the minimum salt cavity depth required would be 1200 m, while the maximum salt cavity depth would be the same as usually recommended for CAES or natural gas storage, 2500 m to avoid salt plasticity at high temperatures (Allen and Doherty, 1982).

For salt cavity scenarios, the most relevant parameters related to the subsurface component are the pressure and temperature conditions, both in the charging phase (well operating as injection) and in the discharge phase (well back-producing CO_2). Using the salt cavity model Khaledi et al. (2016)

$$\rho_a(C_a - R)\dot{T}_a + \frac{\dot{m}_{in}c_a}{V}(T_a - T_{in}) + \frac{RT_a}{V}(\dot{m}_{out} - \dot{m}_{in}) + \frac{h_c A_c}{V}(T_a - T_s)$$

and the wellbore detailed in Appendix 1, the average values of in the salt cavity and the pressure loss in the back-producing well can be obtained. Main assumptions considered in salt cavities modelling:

- The cavern is considered as a single volume.
- The compressibility of the rock salt is very low compared to the compressibility of the gas (V_{Cavern} = Constant).
- During injection and extraction, the mass flow rate is controlled by the operators and the properties of the CO_2 are known.
- The pressure, temperature and density of the CO_2 are uniform over the entire volume of the cavern volume (average pressure and temperature considered inside the cavern).
- The inflow and outflow are steady flow processes (constant flow velocity).
- Storage lithostatic pressures in the salt cavity (P_{max} = 0.8 lithostatic pressure & P_{min} = 0.3 lithostatic pressure; to maintain the cushion gas).
- CO_2 is considered to be an ideal gas.

Limitations in salt cavities model:

- Thermodynamic study neglects the presence of brine in the cavity during injection and withdrawal operations;
- Not considering the impact of this phase on the thermodynamic conditions of the storage, nor even mass and heat exchanges that can occur with the stored fluid;
- Could be studied in task 2.3 (numerically);
- Also neglected possible long term geomechanical effects on salt.

2.2.1 Interfacing salt cavities / surface components

The integration of the salt cavity model and the surface storage system is realized by including the CO_2 injection and production methodology described in the behaviour of the surface CO_2 transcritical cycles defined in Python. This model relies on the CoolProp library [17] for the calculation of substance properties.

In the same way as in the methodology described in deliverable 3.1, to quantify the efficiency of the charging (η_{HP}) and discharging (η_{HE}) phases separately, the impact of using the open-cycle mode of operation, and the roundtrip efficiency (η_{TEES}), the efficiency indicators of equations below are defined.

$$(1)\ \eta_{HP}{}^{*} = \eta_{HP} \cdot \frac{h_{char}}{h_{char,tot}} + \frac{\dot{Q}_{HT-hx,charging}{}^{*} + \dot{Q}_{LT-hx,charging}{}^{*}}{\dot{W}_{C}{}^{*} - \dot{W}_{Exp}{}^{*}} \cdot \frac{h_{char}{}^{*}}{h_{char,tot}}$$

$$(2)\ \eta_{HE}{}^{*} = \eta_{HE} \cdot \frac{h_{dis}}{h_{dis,tot}} + \frac{\dot{W}_{T}{}^{*} - \dot{W}_{Comp}{}^{*}}{\dot{Q}_{HT-hx,discharging}{}^{*} + \dot{Q}_{LT-hx,discharging}{}^{*}} \cdot \frac{h_{dis}{}^{*}}{h_{dis,tot}}$$

$$(3)\ \eta_{ETES}{}^{*} = \frac{(\dot{W}_{T} - \dot{W}_{P}) \cdot h_{dis} + (\dot{W}_{T}{}^{*} - \dot{W}_{Comp}{}^{*}) \cdot h_{dis}{}^{*}}{(\dot{W}_{C} - \dot{W}_{HydT}) \cdot h_{char} + (\dot{W}_{C}{}^{*} - \dot{W}_{Exp}{}^{*}) \cdot h_{char}{}^{*}}$$

where $\dot{Q}_{HT-hx}$ and $\dot{Q}_{LT-hx}$ refer to the thermal power in the high and low-temperature exchanges for each phase, charging and discharging. $\dot{W}$ is the power developed by the compression and expansion equipment, compressor (C), pump (P), expansion in charging (HydT) and gas turbine in discharging (T). The variable " t " refers to the operation time in each phase. The indicators depend on the number of hours in which the system operates in closed or open cycle; h_{tot} would be the total hours of charging (char) and discharging (dis), adding those that the system operates in each mode, the superscript "*" refers to the use of the open cycle operation mode, and $\dot{W}_{Exp}{}^{*}$, $\dot{W}_{Comp}{}^{*}$ would be the expansion power in charging and compression power in discharging, respectively.

Appendix 2 details the approach to integration of the surface and subsurface components of the CEEGS concept in this specific scenario.

2.3 APPROACH TO SENSITIVITY ANALYSIS

The aim of the sensitivity analysis study is twofold. First, we aim at determining which parameters influence results. Second, we also focus on the extent of an effect parameters have on results. For this purpose, first the geological parameters to analyse are selected based on deliverable D2.1 and literature study in each geological scenario. After that, the range of values to analyse are constrained, i.e., their base case, minimum and maximum values. Finally, the results to analyse are determined such as parameters characterizing the efficiency and sustainability of the system. These are defined in Section 2.4.

CMG CMOST tool allows two approaches for conducting sensitivity studies. In one parameter at a time (OPAAT) approach, each parameter is analysed independently while remaining parameters are set to their base value. As a result, the effect of each parameter on the studied variables (results) can be plotted on tornado diagrams. In an alternative approach, multiple parameters are adjusted at the same time and the results are analysed by fitting a so-called response surface to them. It is a proxy for the reservoir simulator that allows fast estimation of sensitivity.

The former technique can be more accurate, but it is computationally more expensive. Since calculation time linearly depends on the number of grid cells, therefore, the sensitivity analysis of parameters using the OPAAT method is eligible for generic geological scenarios where models consist of much less grid cells than site-specific ones.

2.4 METRICS FOR EFFICIENCY AND SUSTAINABILITY

The sensitivity of geological parameters on system performance are studied via metrics characterising efficiency and sustainability. Since the porous media scenarios include reservoir and wellbore models, but plant processes on the surface are not considered, net efficiency metrics such as round-trip and isentropic efficiency cannot be determined at this stage of the project (Oldenburg and Pan 2013).

However, gross efficiency may be used that allows comparing the various (porous) geological scenarios in this respect. Based on similar parameter for compressed air energy storage (CAES) system by Oldenburg and Pan (2013), we define gross efficiency (E_{gross}) that as:

$$E_{gross} = \frac{(m \cdot h)_{w,p}^{discharge}}{(m \cdot h)_{w,i}^{charge}} \times 100$$

That is, E_{gross} is the product of mass flow rate (m) and enthalpy (h) at the wellhead of the production well (w, p) in the discharge phase by the product of mass flow rate and enthalpy at the wellhead of the injection well (w, i) in the charge phase.

Metrics from reservoir engineering such as well productivity and injectivity index are also employed. Since several energy storage cycles with alternating injections and productions must be considered, we employ the average productivity index, PI_{avg}, as defined by Okoroafor et al. (2022) originally for underground hydrogen storage:

$$PI_{avg} = \frac{M_{ProdCO_2}/t}{\left(P_{wr}^2 - P_{wf}^2\right)}$$

where $M_{ProdCO2}$ is the cumulative CO_2 mass produced for all cycles, t is the number of days of CO_2 production, P_r is the static bottomhole (reservoir) pressure and P_f is the flowing bottomhole pressure during production. In the denominator, the difference of squared pressures over the storage cycles are calculated. Note that the parameter has a dimension of mass/time/pressure^2.

Analogously, we define the average injectivity index, II_{avg}, as

$$II_{avg} = \frac{M_{InjCO_2}/t}{\left(P_f^2 - P_r^2\right)}$$

where M_{InjCO2} is the cumulative CO_2 mass injected for all cycles, t is the number of days of CO_2 injection. In the denominator, the difference of squared static bottomhole (reservoir) pressure, P_r, and the flowing bottomhole pressure during injection, P_f, are considered.

Furthermore, implication for long term behavior of the system is quantified by comparing the average injectivity index with the average productivity index, i.e., taking their ratio defined as sustainability index, SI:

$$SI = \frac{II_{avg}}{PI_{avg}}$$

As the index suggests, if SI is close to 1, injection and production of CO_2 are in balance, otherwise either more CO_2 is injected into the reservoir than produced, i.e., $SI>1$, or vice versa, $SI<1$ during the energy storage cycles. Since the CEEGS concept aims at delivering the advantages of CCS and energy storage systems, thus, if $SI>1$, the CO_2 sequestration feature of CEEGS may is dominant, which will maximise the economic favourability. However, if $SI<1$, the energy storage component is dominating.

In the geothermal scenario, an additional metric, heat extraction is introduced, which is defined as the wellhead temperature difference between injector and producer during discharge cycle (see well configuration in Section 3.4). As its name implies, the larger the wellhead temperature difference, the more heat can be extracted from the reservoir.

3 SCENARIO DESCRIPTION AND RESULTS

3.1 BASE SCENARIO: DEEP SALINE AQUIFER, OPEN BOUNDARIES

3.1.1 General description

The Deep Saline Aquifer (DSA) with open boundaries is the **Base Case Scenario**. It is an 'open' boundaries porous media aquifer, in which there are no lateral constraints (such as impermeable boundaries) to the migration of CO_2 and brine within the pressure build up zone imposed by the injection well. That is, hydraulically the DSA is considered as 'infinite'.

Furthermore, the base case scenario includes an anticline structure as a structural trap (Figure 3). It is based in the PilotSTRATEGY Lusitanian basin case, Portugal, in which the reservoir is the Lower Cretaceous sandstone from the *Torres Vedras* Group (Wilkinson et al. 2023).

This base case scenario includes five variants:

- Three variants aim to test the relevance of reservoir depth to the efficiency of the CEEGS technology. i) **Variant "850m"** referring to the average top reservoir depth below. It is the actual PilotSTRATEGY scenario; ii) **Variant "+1000m"** in which the average top reservoir depth is 1850m below surface, and; iii) **Variant "+2000m"** in which the average top reservoir depth at 2980m below surface. In all these variants the reservoir is homogeneous;
- Two variants aim to study the effects of spatial (heterogeneity) and directional (anisotropy) variations in permeability: iv) **Variant "Heterogeneity"** and; v) Variant "Anisotropy" in permeability. These variants are further described in Appendix 3, part A.

The model geometry and well configuration is similar for all variants.

3.1.1.1 Gridding and input parameters

Figure 3 shows the original PilotSTRATEGY geological model, much larger than required for this analysis, the extracted sub-model used in CEEGS and the refined grid around wells.

The size grid of the reservoir model used is 250m×250m×20m. The grid elements in the target area and near the borehole are refined into a regular cartesian grid to improve the computational accuracy, with grid block size of 20m×20m×6m in x, y, z directions respectively. The key reservoir and wellbore parameters used in the simulation model are outlined in Table 2 and Table 3. The permeability of the aquifer is 300mD and the porosity of the aquifer is 0.15, representing a homogeneous and isotropic base case. The average thickness of the reservoir is 340m.

CO_2/brine properties and the partitioning features (i.e., equilibrium k values) are calculated using Redlich– Kwong (RK) equation of state (Redlich and Kwong, 1949; Hassanzadeh et al. 2008). The gas/water relative permeability curves were constructed using the Brooks–Corey correlations (Brooks and Corey, 1964).

The caprock is assumed to have suitable conditions for CO_2 storage and is not specifically modelled in any of the scenarios.

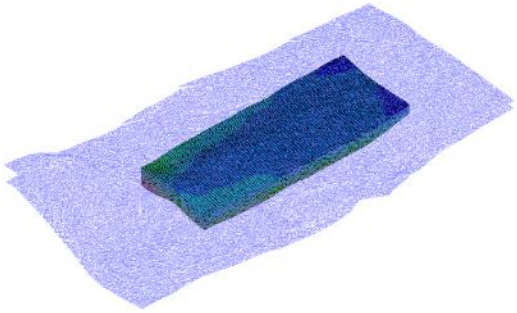

(a) Original model domain

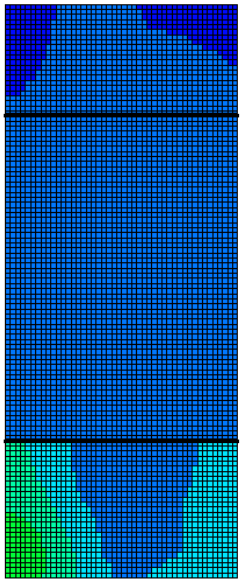

(b) Top view and the limits of the extracted sub-model

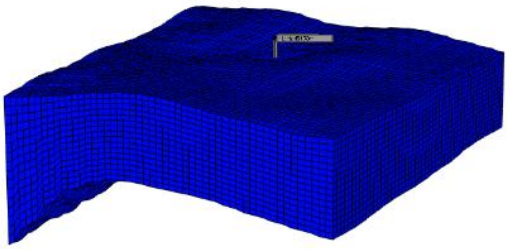

(c) Extracted 3D sub-model

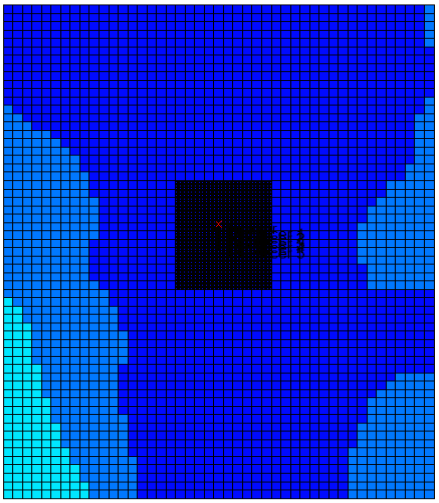

(d) Areal view of the extracted sub-model with refined zone near the wells

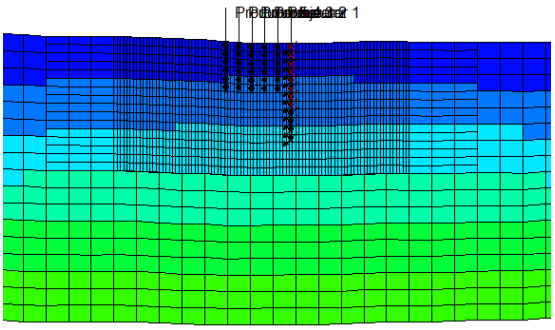

(e) Reservoir cross section and well location

Figure 3: Reservoir modelling domain, extracted sub-model, and refined well region.

Table 2: Reservoir properties**.**

Property	Value	unit
Average aquifer thickness (m)	340	
Porosity	15	(%)
Permeability (mean)	300	mD
Vertical anisotropy Kv/Kh	1	-
Brine density	1025	Kg/m^3
Reference depth	854	m
Pressure at reference depth	$P= P_{atm}+\rho_w gZ$	Kpa
Maximum Bottomhole pressure	Static pressure+20%	Kpa
Initial aquifer temperature	$T=T_s+GZ$	ºC
Rock compressibility	$4.2E^{-6}$	Pa^{-1}
Rock-fluid: parameters for relative permeabilities		
Residual gas saturation	0	-
Connate water saturation	0.25	-
Rock thermal properties		
Volumetric heat capacity	$Cp = 1.2\times10^6$	$J/m^3.C$
T-dependent coefficient	2.85×10^3	
Rock thermal conductivity	2.47×10^5	J/m.day.C
Geothermal gradient (GZ)	0.03	(ºC/m)
H_2O thermal conductivity	5.35×10^4	J/m.day.C
Gas thermal conductivity	4500	J/m.day.C
Surface temperature	15	ºC

Table 3: Well geometry and thermal parameters used in the simulation.

Properties	Value	Unite
Wellbore properties		
Wall heat capacity	3.63×10^6	$J/m^3.C$
Wall thermal conductivity	3.888×10^6	J/m.day.C
Thermal properties of cement		
Heat capacity	1.848×10^6	$J/m^3.C$
Thermal conductivity	118 400	J/m.day.C
Thermal properties of insulation		
Heat capacity	3283	J/m^3 -C
Thermal conductivity	16 800	J/m.day.C
Relative roughness	0.0001	
Wellbore		
Tubing	298.4 OD/281.1 ID	mm
Casing	339.6 OD/322.8 ID	mm

3.1.1.2 Initial and boundary conditions

The initial fluid pressure was set to hydrostatic. The initial reservoir temperature was set by considering a linear dependence on the geothermal gradient (30 °C Km^{-1}) and a surface temperature of 15°C. The initial water and gas saturations of the reservoir are 1 and 0, respectively. Cell volume modification is used at the four side boundaries to represent open boundaries to flow and heat transfer. Figure 4 depicts the initial pressure and temperature conditions. The model was run for 500 years, without any CO_2 injection, to ensure steady-state conditions exist before the first stage of CO_2 injection – plume setup. Similar procedures were followed for all other variants.

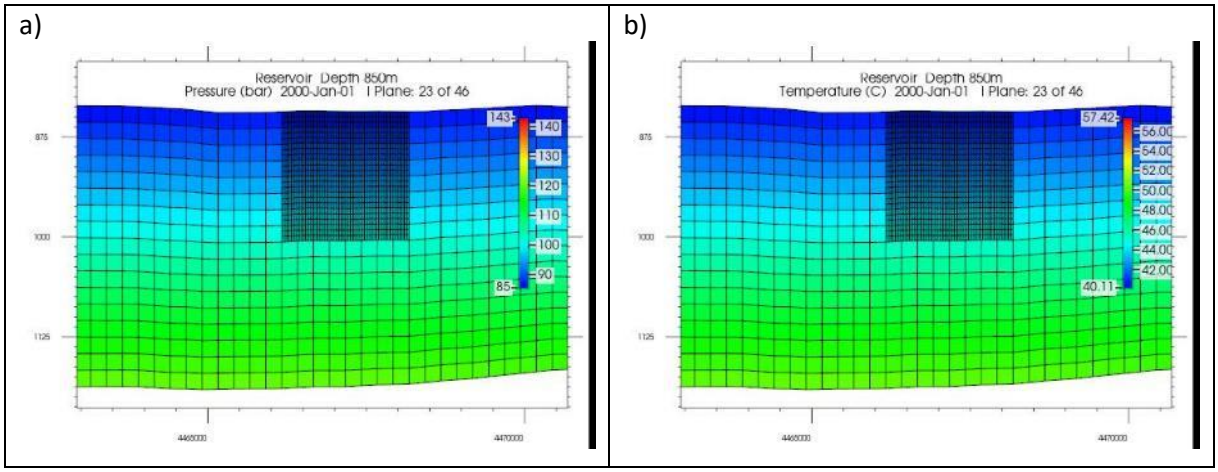

Figure 4: Initial conditions in the "850m" variant in section view. a) pressure; b) temperature.

3.1.1.3 CO_2 injection and initial plume setup

Because the CEEGS system does not favour thick reservoirs (see deliverable D2.1), during the plume setup stage, CO_2 was injected into the aquifer at the top third of the reservoir's thickness. Figure 5 illustrates the spatial distribution of gas saturation, temperature, and pressure within the reservoir after two years of injection. The CO_2 plume has a quasi-radial shape, due to the homogeneity of rock properties and the plume at the top of the reservoir can stretch over 1000 meters.

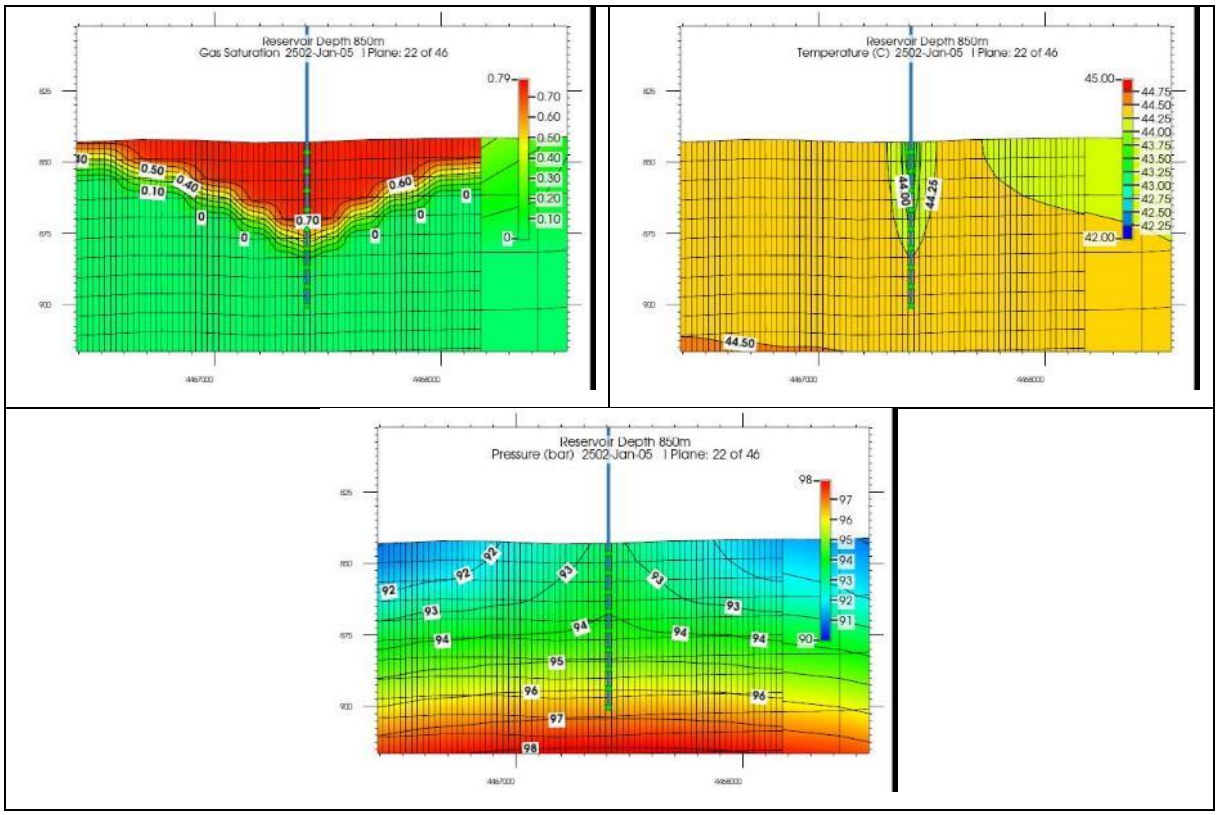

Figure 5: Spatial distribution of gas saturation, temperature (°C), and pressure (bar) around injection Well A after 2 years of continuous injection. Section view.

The area closer to the injection Well A is slightly cooler than the rest of the reservoir, since the CO_2 temperature at the injection wellhead was set to 20°C (the CO_2 is directly supplied from the stationary capture plant) but the difference is small, since the CO_2 tends to equilibrate to the reservoir temperature as it ascends to the top of the reservoir. The area around the injection Well A shows higher pressure due to the injection process, but caution was taken to ensure sure that bottomhole pressure does not exceed the hydrostatic pressure by more than 20%. This minimises the risk of fracturing the reservoir and the caprock. The results of the CO_2 plume setup for the two other reservoir variant depths scenarios are shown in Figure 6.

The results for the simulation of charge/discharge cycles and the sensitivity analysis can be found in Appendix 3, part A.

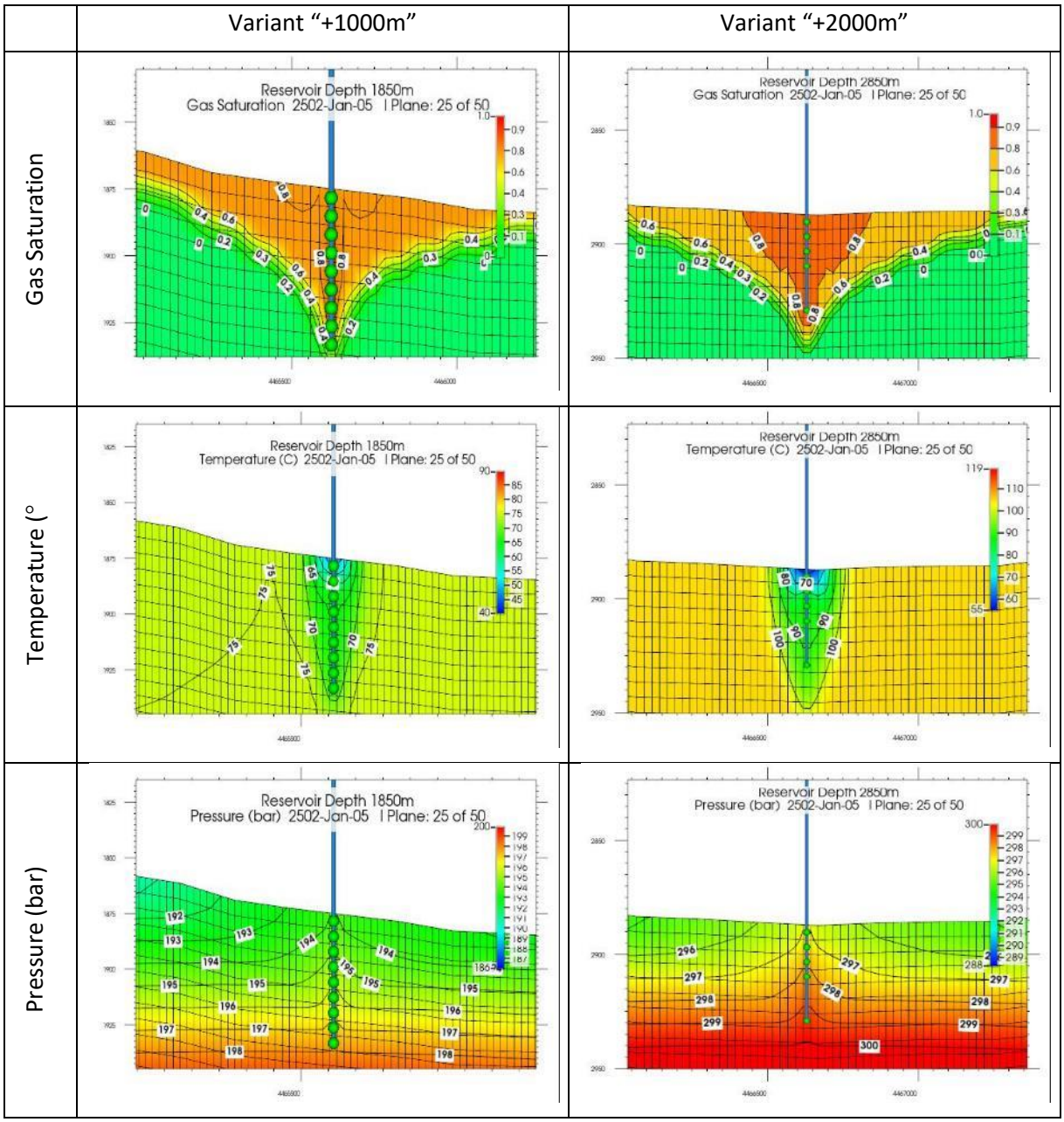

Figure 6: Spatial distribution of gas saturation, temperature (°C), and pressure (bar) around injection Well A after 2 years of continuous injection for the Variant "+1000m" (left) and the Variant "+2000m" (right). Section view.

3.2 SCENARIO II: DEEP SALINE AQUIFER, CLOSED BOUNDARIES

3.2.1 General description

In this scenario, the geological reservoir is a closed deep saline aquifer (DSA) with the presence of faults acting as lateral impermeable boundaries. The aim goal of this scenario is to study pressure buildup, plume size and long-term plume migration under conditions in which the brine in the DSA cannot migrate from the geological structure. The injection rate is the same as for the open reservoir aquifer (33kg/s) , but to address the uncertainty on the amount of CO_2 injected to the buildup pressure, a flowrate of 10kg/s with a period of one year of continuous injection is used as a variant case.

The geological setting is provided by a Buntsandstein sandstone reservoir in northern Spain. The reservoir is composed of three units of 63 layers of distinct properties, varying from 1887m to 2021m deep. The upper, intermediate and the lower unit (the target reservoir) show average permeability values of 50, 100 and 500 md respectively, and a porosity of 0 (which is considered as the caprock of the reservoir), 8% and 12%. The pore compressibility for all formations was assumed to be 4.2×10^{-10} Pa^{-1}.

3.2.1.1 Gridding and input parameters:

The model domain was defined so that boundary effects on the pressure buildup and CO_2 plume are significant during the plume setup stage and the charge-discharge cycles. The numerical simulation model is 11 km×10 km reservoir with a discretisation of 200m×200m×2 m in x, y, z directions, the sub-model is cut from the larger 3D geological model (Figure 7). A grid refinement has been performed around the wells to improve results accuracy and to ensure that the cell sizes were sufficient to capture the behaviour of CO_2 while minimizing computational time**.**

The refined zone region is 1.4km×1km and it is bounded by two faults, with a cartesian grid 50m×50m×2m in x, y, z directions respectively (Figure 7). In the vertical direction, the target zone is composed of 38 layers of 120m thickness with a cell thickness of 2m in the z-direction. The perforation interval was set to 33% of the reservoir thickness for the injection phase in Well A and Well B (both charge and discharge phases), however for the discharge phase of producer Well A, the perforation is set to top of reservoir (about 14 m) to limit the brine production.

3.2.1.2 Initial and boundary conditions

The initial hydrostatic pressure was calculated based on the water density (water salinity of 1025 kg/m^3) and the reservoir depth. Initial temperature distribution was computed from the surface temperature of 15°C and linear temperature gradient of 30°C Km^{-1}). The model was run for 500 years to reach steady state pressure and temperature, and the outcome of that run was used as the initial conditions for the CO_2 plume setup stage.

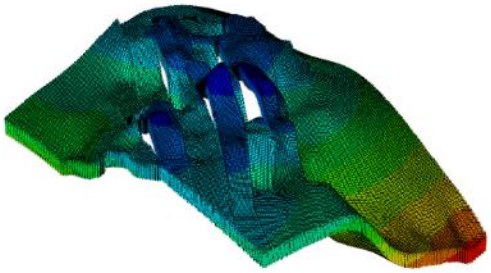

(a) Full model domain compartmentalised by faults. Vertical scale is exaggerated.

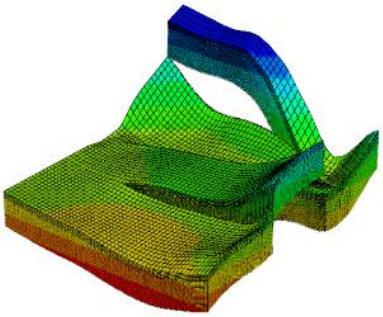

(b) Extracted sub-model, compartmentalised by 3 faults. Vertical scale is exaggerated.

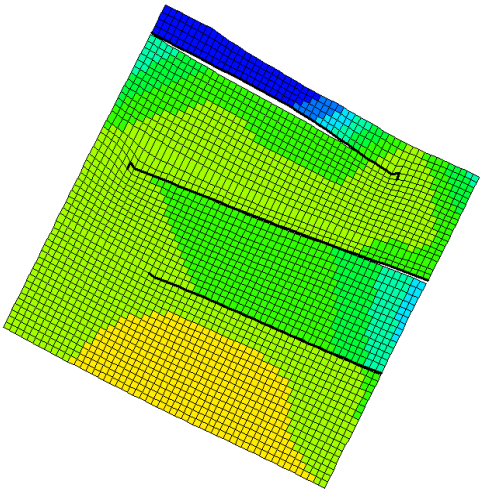

(c) Top view of the sub-model

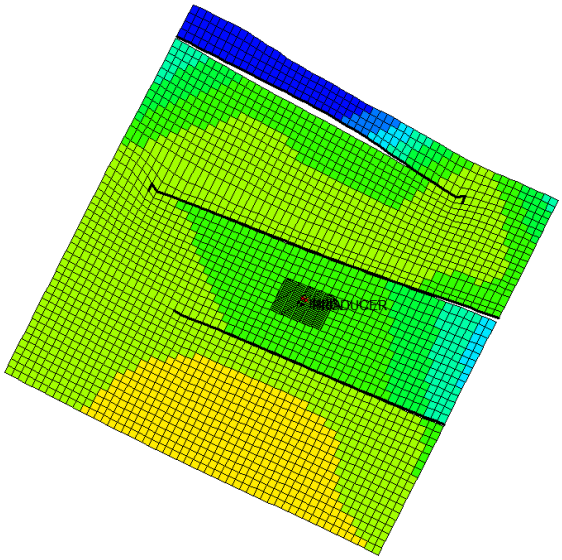

(d) Areal view of the extracted model with refined zone near the wells. Black lines are faults.

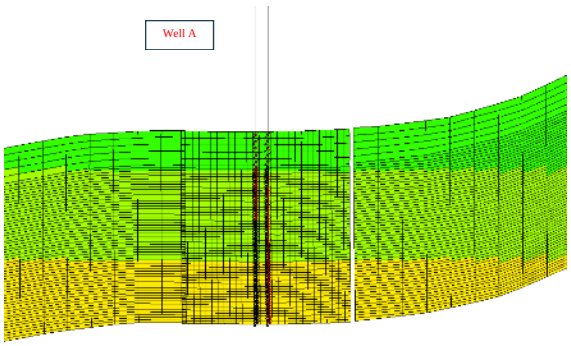

(e)Reservoir cross section and well location

Figure 7: Model domain, extracted sub-model, and refined well region.

3.2.1.3 CO_2 injection and initial plume setup

Figure 8 shows a spatial distribution of the CO_2 saturation within the reservoir layers throughout two years of continuous injection. The reservoir comprises three distinct layers, each characterized by varying permeability and porosity parameters. The upper layer, the caprock, exhibits low permeability (10^{-4} mD) and possesses negligible porosity in order to simulate an impermeable caprock. Subsequent to the caprock, an intermediate layer emerges with a permeability of 100 mD and a porosity of 0.08, as depicted in Figure 8. Finally, the lower layer, which with a porosity of 0.12 and a permeability of 500 mD. This layer stands out as particularly high permeable for CO_2 flow compared to the second layer, rendering it the designated injection point for the CO_2. However, owing to its lower density, the migration of CO_2 from the third layer into the second layer occurs, ultimately accumulating just beneath the caprock, as illustrated in Figure 8. This migration results in the absorption of heat, and the CO_2 attains an equilibrium temperature of 75°C.

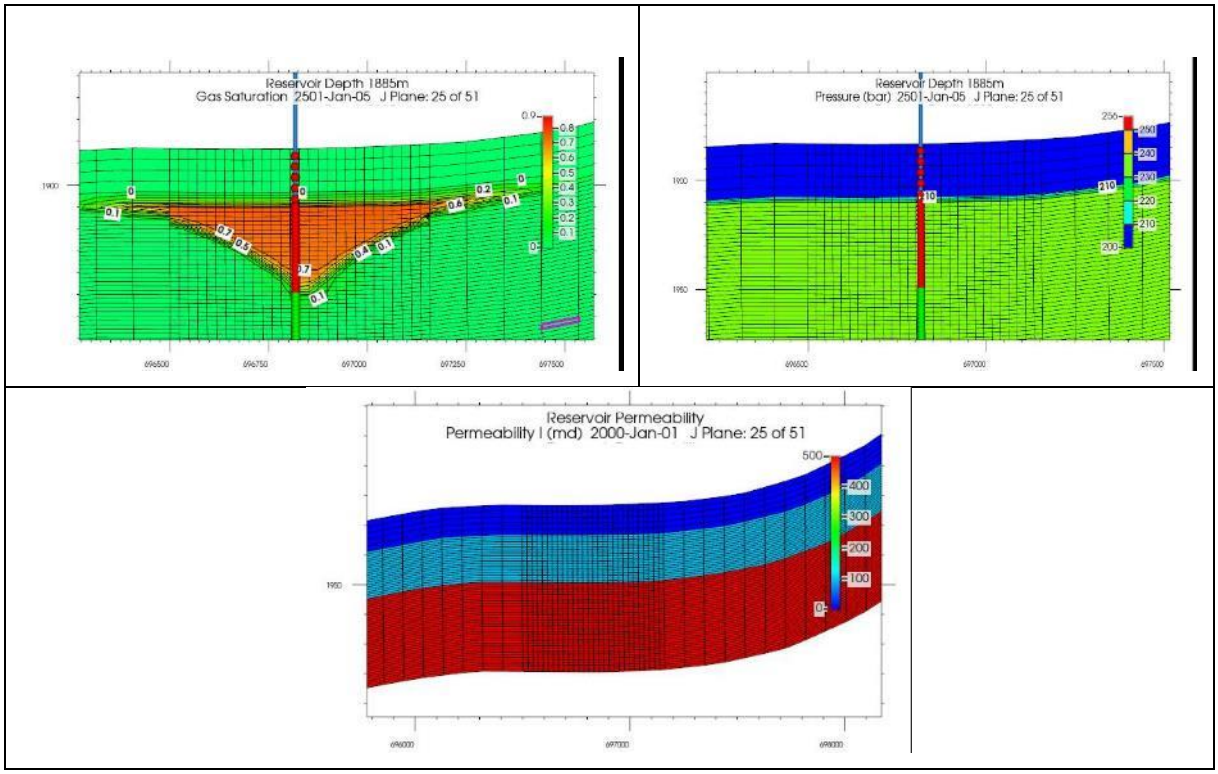

Figure 8: Section view of gas saturation, pressure and temperature during the plume setup stage (1 year of CO_2 injection).

Figure 8 was built with an injection rate of 10 kg/s. In fact, to prevent hydraulic fracturing of the target formation and caprock, we conducted a comparison between the simulated pressure buildup (ΔP) and the critical pressure buildup (ΔP_f), set as 20% of the hydrostatic pressure. Given the depth of the reservoir, which is approximately 2022 meters, the calculated critical pressure buildup amounts to 40 bars. Consequently, we employed a critical fracturing pressure of ΔP_f = 204.5 bars + 40 bars (overpressure), resulting in a total of 245 bars, for the purposes of this study.

Figure 9 (a) presents the BHP profile in Well A, illustrating the pressure evolution during the 2-year plume setup stage.

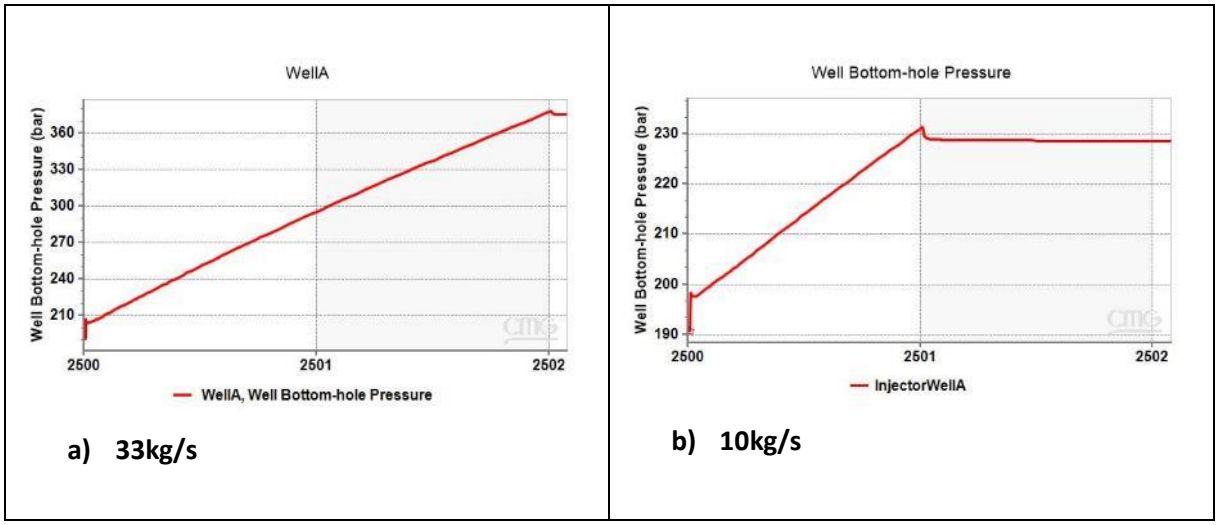

Figure 9: BHP in Well A during the plume setup stage: a) 33kg/s for 2 years of continuous injection, b) 10kg/s for 1 year of continuous injection.

After 6 months of injection, the pressure at the injection well reaches the boundaries of the model. Upon cessation of injection after 2 years, the BHP surpasses the reservoir's fracturing pressure limit by 120%. This indicates that the desired flowrate of 33 kg/s violates the bottomhole pressure limit, leading to the conclusion that this scenario is unfeasible for the considered reservoir. The maximum flow rate permissible to maintain an acceptable BHP is found to be 10 kg/s, sustained over a one-year period during the plume setup stage (Figure 9).

The results for the simulation of charge/discharge cycles and the sensitivity analysis can be found in Appendix 3, part B.

3.3 SCENARIO III: TWO DEEP SALINE AQUIFERS

3.3.1 General description

This scenario investigates the feasibility of the CEEGS concept using two deep saline aquifers at two different depths in two configurations taking advantage of CO_2 thermodynamical properties at various pressure-temperature conditions.

As pointed out in deliverable D2.1, a similar concept is suggested by Liu et al. (2016) and Fleming et al. (2022). These studies hint at the possibility that two porous media reservoirs at different depths can be used for implementing the CEEGS concept. Based on that deliverable, we employ the following two configurations that are summarized below.

In the first configuration, referred to as **transcritical CO_2 (TC-CO_2) case**, the upper reservoir is located at a depth such that CO_2 remains in gaseous phase throughout the energy storage cycles. Moreover, this depth is as high as possible (as far as possible from surface) in order to comply with potential environmental regulations. The bottom reservoir is located at much larger depth.

In the other configuration, defined as **supercritical CO_2 (SC-CO_2) case**, the upper reservoir is located at a depth that ensures storing and producing CO_2 in supercritical conditions throughout the energy storage cycles.

In both system configurations, CO_2 is injected in both reservoirs at the same time to establish cushion gas. The injection rate is controlled by the imposed condition on wellbore bottomhole pressure that is not allowed to exceed 20 % of the hydrostatic (reservoir) pressure to ensure storage security. In this way, no additional geomechanical analysis of caprock integrity is required at this stage of the project. The plume establishment period is maximized in two years for practical reasons. This will be investigated and optimized in great detail in deliverable D3.2.

After the plume establishment phase, the 24-hour-long energy storage cycles are maintained for 6 days where discharge and charge cycles are realized as follows.

3.3.1.1 Gridding and input parameters

The reservoir configuration where CO_2 is circulated in gaseous phase in the upper reservoir is simulated using quasi-isothermal CMG-STARS since the non-isothermal numerical solver of CMG-GEM cannot converge if gaseous and supercritical phase transitions within one configuration are simulated. The quasi iso-thermal condition is realized by having one-one temperature value defined for the upper and bottom reservoir according to geothermal gradient typical for the Pannonian basin. Based on the simulation of CO_2 sequestration into shallow saline aquifer in Ketzin, Germany, storing CO_2 in gaseous phase or close to supercritical condition, isothermal simulation conditions can provide good agreement with field record (Kempka et al., 2010). However, this may be not the case for the bottom reservoir, where CO_2 in supercritical condition can be assumed. Since supercritical CO_2 viscosity and density show large variation even to small pressure and temperature variations, thus, the validity of that part of the results must be checked against other (analytical) tools in the future.

The other reservoir configuration, where CO_2 is stored and produced in supercritical phase in the upper reservoir, is simulated using non-isothermal CMG-GEM simulator.

The numerical grid for the reservoir configuration with gaseous CO_2 is illustrated in Figure 10 and that with $ScCO_2$ is illustrated in Figure 11. In both cases, the models have a size of 2000 m x 2000 m and a total thickness of 1300 m. The models consist of 96.000 cells, with grid block size in the horizontal direction is 50 m, and the vertical cell size in the reservoirs is 10 m and in the upper caprock is 40 m. The cell size in the bottom caprock is different in the two configurations, with 230 m for the gaseous CO_2 case and 100 m for the $ScCO_2$ case. The caprocks have coarser vertical grid cell since we do not pay special attention to them at this stage of the investigation. The reservoirs have a thickness of 200 m.

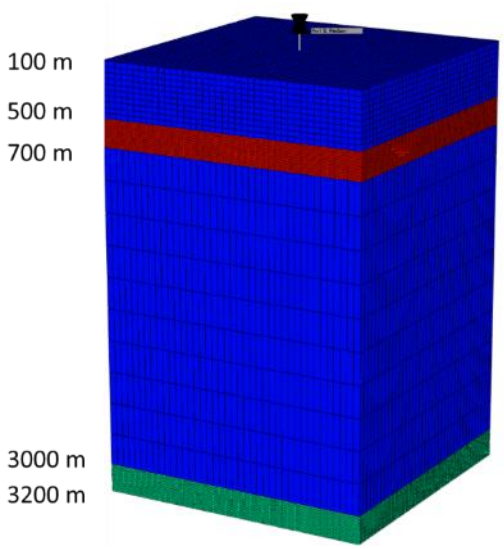

Figure 10: Numerical grid of the two deep saline aquifer scenario, illustrating upper reservoir (red cells) and bottom reservoir (green cells) and impermeable caprock (blue cells).

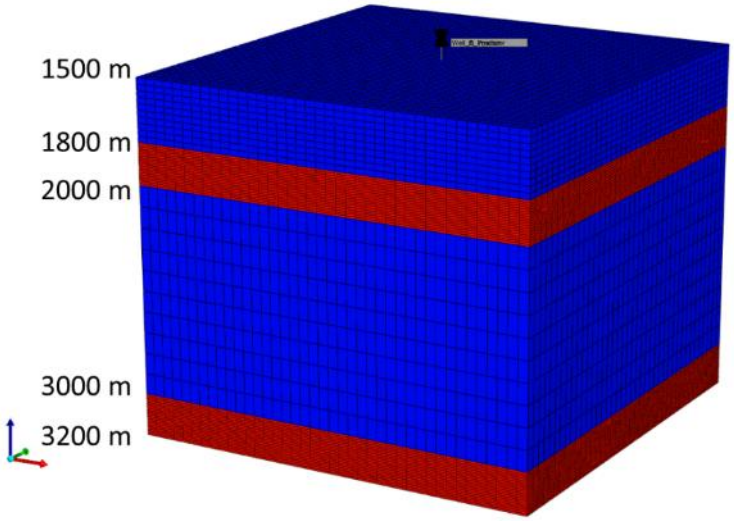

Figure 11: Numerical grid of the two deep saline aquifer scenario, illustrating upper reservoir and lower reservoir (red cells) and impermeable caprock (blue cells).

The petrophysical parameters of the generic models is based on Pannonian sandstone of the Pannonian Basin. Pannonian sandstone formations have been used for geothermal purposes, hydrocarbon production as well as natural gas storage since decades (Tóth et al., 2018; Koroncz et al., 2022). Therefore, this geologic environment does not only provide basis for populating the generic geological scenarios but can be later used for optimization purposes in WP3.

The initial input parameters including their base case, minimum and maximum value and reference are summarized in Table 4. Regarding permeability and porosity, we aim at reflecting larger values at shallower depths as expected for lower level of compaction as reported by Horváth et al. (2015) and Koroncz et al. (2019).

Table 4: Grid parameters for the two deep saline aquifer scenario with two variants, transcritical CO_2 (TC-CO_2) and supercritical CO_2 (SC-CO_2).

Parameter	Value TC-CO_2 variant	Value SC-CO_2 variant	Reference
Horizontal permeability in upper reservoir (mD)	500	200	Horváth et al. (2015); Koroncz et al. (2022)
Horizontal permeability in bottom reservoir (mD)	200		
Horizontal/vertical Permeability ratio	3		
Geothermal gradient (°C/km)	-	40	Lenkey et al. (2021)
Porosity in upper reservoir (%)	20	15	Koroncz et al. (2022); Willems et al. (2021)
Porosity in bottom reservoir (%)	8	8	
Salinity (mg/l)	15000		Tóth et al. (2018); Varga et al. (2019)
Relative permeability & capillary pressures	Basal Cambrian Sandstone		Bennion and Bachu (2005); Bennion and Bachu (2006)

In both configurations, caprock is defined as impermeable with low porosity. Furthermore, since no relative permeabilities and capillary pressures are available for this rock type, we use values reported by Bennion and Bachu (2005, 2006).

3.3.1.2 Initial and boundary conditions

The reservoirs are initially at hydrostatic equilibrium which is defined by constant hydrostatic pressure gradient in the cells. Furthermore, the pore space is assumed to be entirely filled by brine. As for thermal initial conditions, constant temperature gradient is defined, and no heat flow is imposed on the reservoirs.

Regarding boundary conditions, the reservoirs are laterally open which is achieved by defining extremely large cell volume modifiers, i.e. 100.000 in the respective boundary cells resulting in constant pressure values.

3.3.1.3 Equilibrium conditions and initial plume configuration

It is assumed that pure CO_2 is injected at a target rate of 33 kg/s or ~ 1 Mt/year while well bottomhole pressure cannot exceed the hydrostatic pressure by more than 20 %, and the wellhead temperature is 60 °C for both wells.

An overview of the initial engineering conditions for the TC-CO_2 variant is provided in Table 5 . The plume (cushion gas) configuration lasts for 2 years.

Table 5: Summary of input well parameters during plume gas establishment phase for the TC-CO_2

Well	Well radius	WHP (bar)	WHT (°C)	Target Mass rate (kg/s)	Target BHP (bar)
Well A	0.2	80	60	33	Hydrostatic ±20%
Well B		50	24		Hydrostatic ±20%

Figure 12 summarizes the simulated well bottomhole pressures (BHP) during the plume setup phase. In the bottom reservoir, the desired mass rate can be achieved within the safety pressure margin. However, in the upper reservoir, the BHP reaches the safety margin level and the maximum injection mass rate at the end of the simulation is approx. the half of the desired value, due to its higher density. Therefore, much less CO_2 is injected in the upper reservoir compared to bottom one.

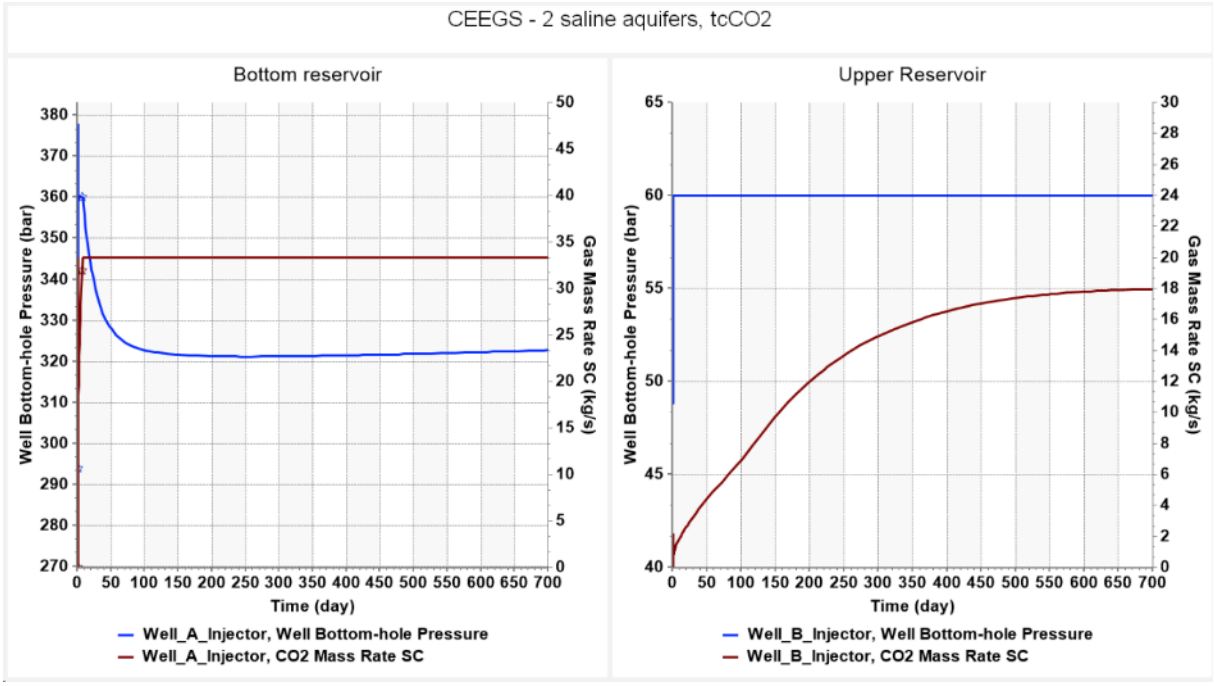

Figure 12: Simulated well bottomhole pressures and mass rates in the bottom and upper reservoir during plume setup period where CO_2 is stored in gaseous phase.

Figure 13 shows the spatial gas distribution at four stages of the simulation. According to that, the plume in both reservoirs reaches model boundaries already after 0.5 year of simulation, but its thickness is much larger in the bottom one.

An overview of the initial engineering conditions for the SC-CO_2 variant is provided in Table 6. The plume (cushion gas) configuration lasts for 2 years.

Figure 14 shows the simulated well bottomhole pressure during the initial plume configuration phase for the SC-CO_2 variant. Throughout the whole setup phase, the maximum pressure does not reach the safety limit neither in the upper, nor in the bottom reservoir, i.e., 228 bar and 360 bar, respectively. Thus, no fracturing hazard is expected in the caprock formations.

The distribution of scCO_2 in the reservoirs is shown in Figure 15. The figure demonstrates that in both reservoirs the extent and thickness of establish plume is large enough to potentially maintain stable charge and discharge cycles.

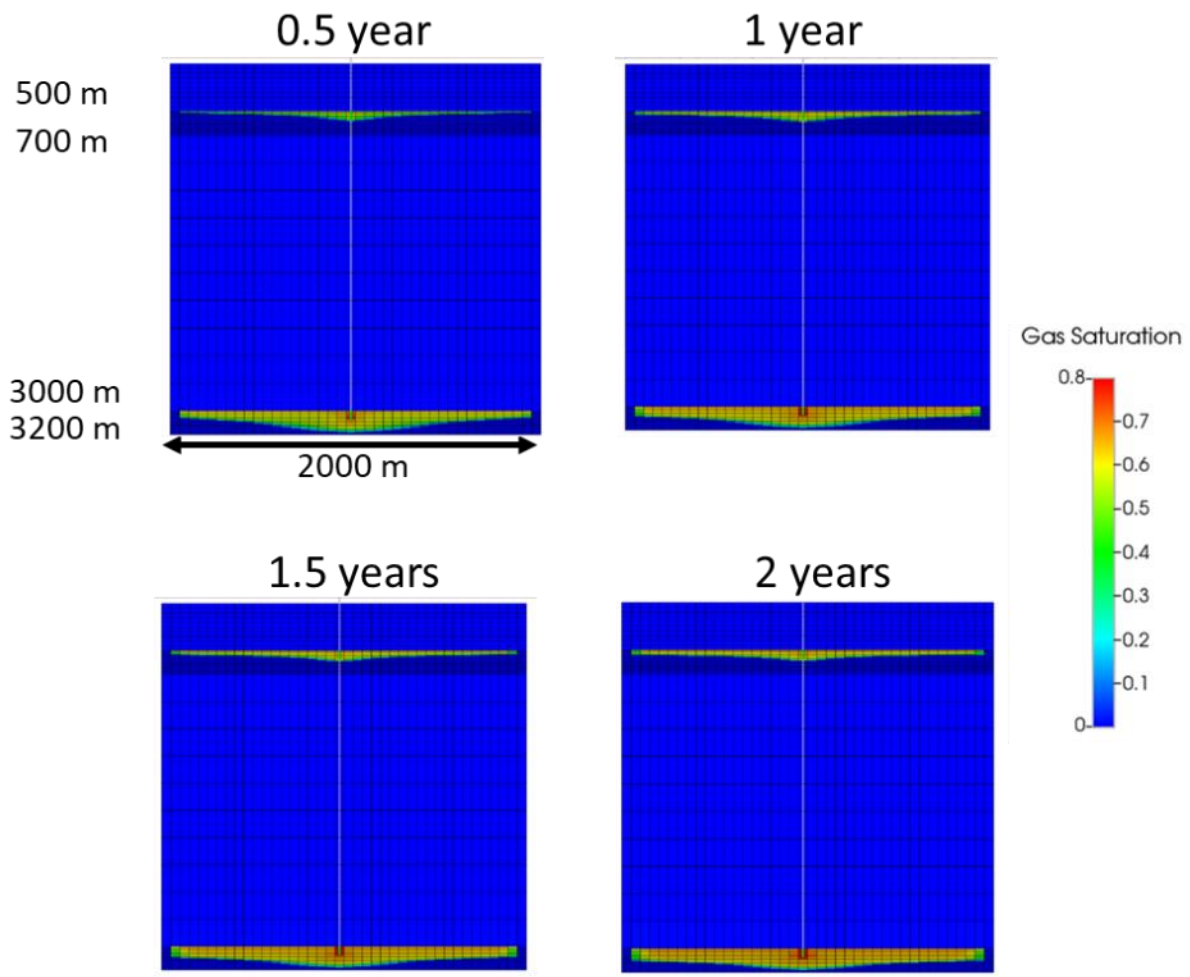

Figure 13: Snapshot of CO_2 saturation distribution in the reservoirs after 0.5, 1, 1.5 and 2 years of onset of injection during the plume establishment phase for the TC-CO_2 variant.

Table 6: Summary of input well parameters during plume gas establishment phase for the SC-CO_2 variant.

Well	Well radius	BHT (°C)	Target Mass rate (kg/s)	Target BHP (bar)
Well A	0.1	97	33	Hydrostatic ±20%
Well B		62.5		Hydrostatic ±20%

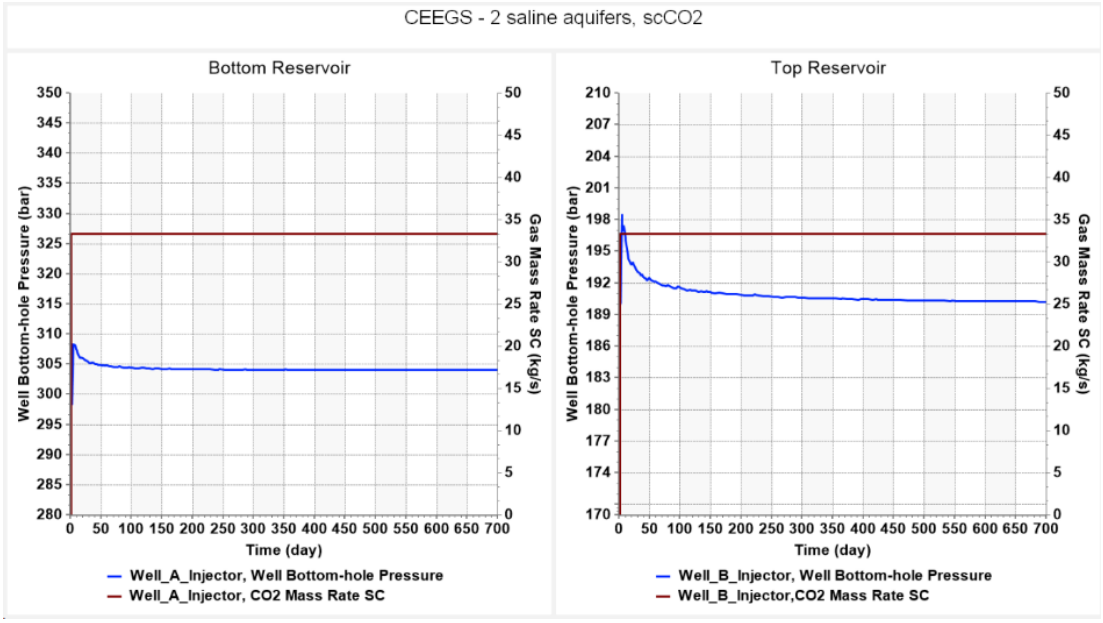

Figure 14: Simulated well bottomhole pressures and mass rates in the bottom and upper reservoir during plume setup period where CO_2 is stored in supercritical phase.

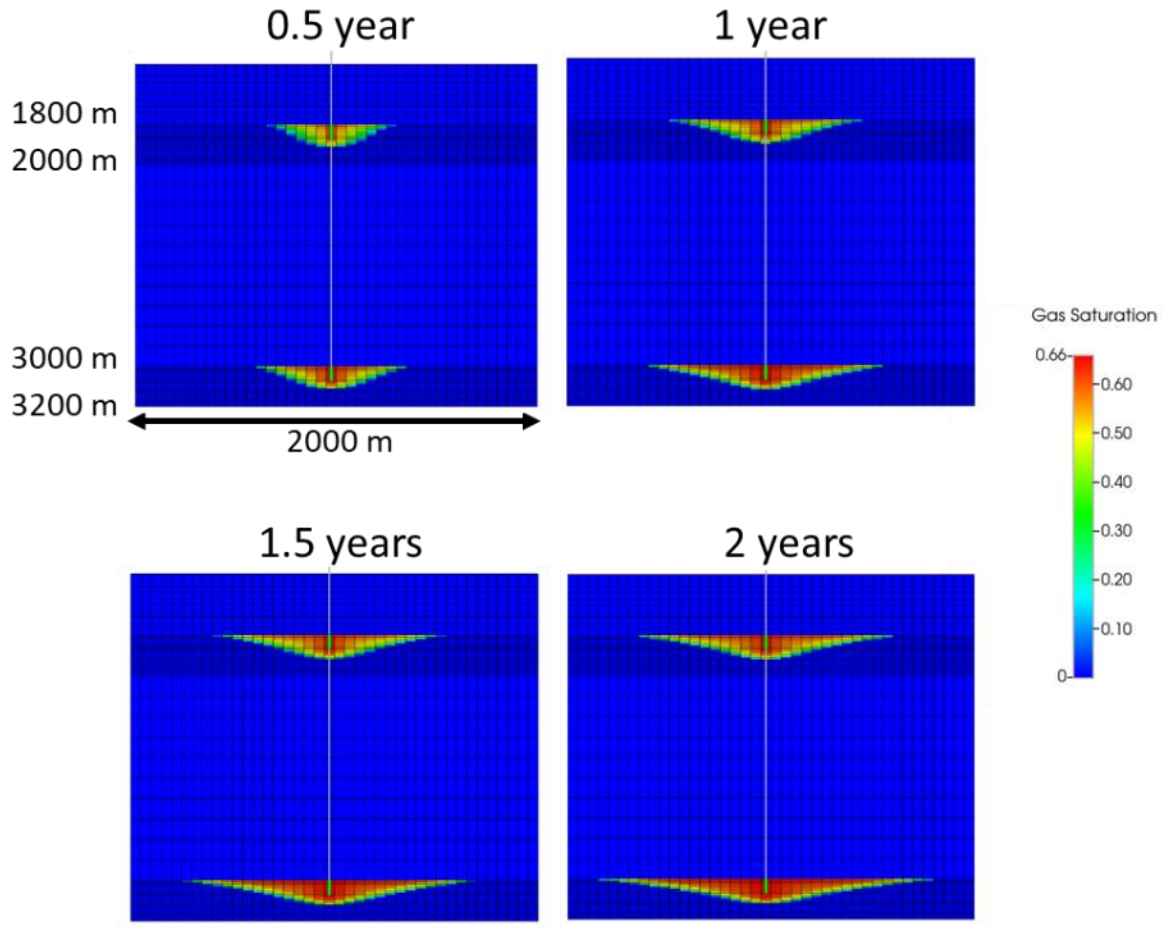

Figure 15: Snapshot of CO_2 saturation distribution in the reservoirs after 0.5, 1, 1.5 and 2 years of onset of injection during the plume establishment phase for the SC-CO_2 variant.

The results for the simulation of charge/discharge cycles and the sensitivity analysis can be found in Appendix 3, part C.

3.4 SCENARIO IV: GEOTHERMAL RESERVOIR

3.4.1 General description

The scenario investigates the feasibility of the CEEGS concept in a generic geothermal reservoir implemented in a carbonate reservoir. The conceptual model is based on a geothermal reservoir located in the geological region Molasse Basin in Southern Bavaria in Germany. In particular, the Munich area is known for several geothermal projects providing either electric power and/or heat for district heating system since several decades (Moeck 2014; Moeck et al. 2019). In this task, the operating Unterhaching hydrothermal system (Knapek and Knittl 2007; Wolfgramm et al. 2007) is used as a basis for the conceptual model due to availability of required information for conducting the simulations such as geological setting, petrophysical data of the reservoir and overburden rock as well as reservoir engineering data (Cacace et al. 2013; Rühaak et al. 2017).

Based on typical hydrothermal systems (Huenges, 2010), geothermal well doublet is assumed.

The short-term, 24-hour-long energy storage cycles are maintained for 6 days where discharge and charge cycles are realized.

3.4.1.1 Gridding and input parameters

The circulation and storage of CO_2 in supercritical phase in the reservoir is simulated using non-isothermal CMG GEM code. The numerical grid is illustrated in Figure 16. The model has a size of 2000 m x 2000 m and a thickness of 200 m. The model consists of 128 000 cells, where grid block size in the horizontal direction is 25 m, and cell thickness is 10 m. The caprock is not simulated explicitly since its mechanical integrity is assumed to be maintained via the injection parameters described below. Therefore, mechanical processes, such as deformation and fracturing processes are not considered. Furthermore, chemical processes, such as salt precipitation are not investigated in this task.

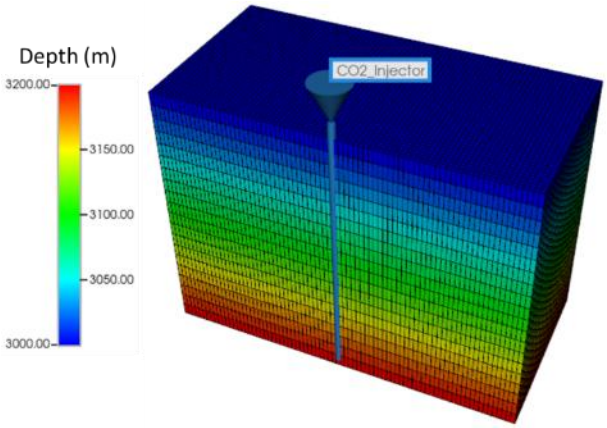

Figure 16: Numerical grid of the carbonate reservoir.

The initial input parameters including their base case, minimum and maximum value as well as reference are summarized in Table 7.

Table 7: Grid parameters of the geothermal carbonate reservoir.

Parameter	Value: base case; minimum; maximum	Data source
Horizontal permeability in reservoir (mD)	100; 50; 1000	Moeck, 2014; Cacace et al. 2013
Horizontal/vertical Permeability ratio	3	
Temperature gradient (°C/km)	40; 35; 45	Rühaak et al. 2017
Porosity (%)	8; 5; 15	Moeck, 2014; Cacace et al. 2013
Salinity (mg/l)	750	Wolfgramm et al. 2007
Relative permeability & capillary pressures	Basal Cambrian Sandstone	Bennion and Bachu (2005); Bennion and Bachu (2006)

The studied reservoir exhibits salinity much lower compared to deep sandstone saline aquifers, therefore its effect in the sensitivity study is not investigated. Given that no CO_2-brine capillary pressures and relative permeabilities are available for the studied rock type, we use values reported for Nisku Carbonate rock from Wabamun Lake area in Alberta, Canada by Bennion and Bachu (2005) and Bennion and Bachu (2006), respectively.

3.4.1.2 Initial and boundary conditions

The reservoir is initially at hydrostatic equilibrium which is defined by constant hydrostatic pressure gradient in the cells. Furthermore, the pore space is assumed to be entirely filled by brine. As for thermal initial conditions, constant temperature gradient is defined, and no heat flow is imposed on the entire reservoir.

Regarding boundary conditions, the reservoir is laterally open which is achieved by defining extremely large cell volume modifiers, i.e., 100.000 in the respective boundary cells resulting in constant pressure values.

3.4.1.3 Equilibrium conditions and initial plume configuration

It is assumed that pure CO_2 is injected at a target rate of 33 kg/s or ~ 1 Mt/year while well BHP cannot exceed the hydrostatic pressure by more than 20 %, and the bottomhole injection temperature is 110°C. The injection is maintained for 2 years.

Figure 17 shows the simulated well BHP during the initial plume setup stage. Throughout the whole setup stage, the maximum pressure does not reach the safety limit, i.e., 375 bar. Thus, no fracturing hazard is expected in caprock.

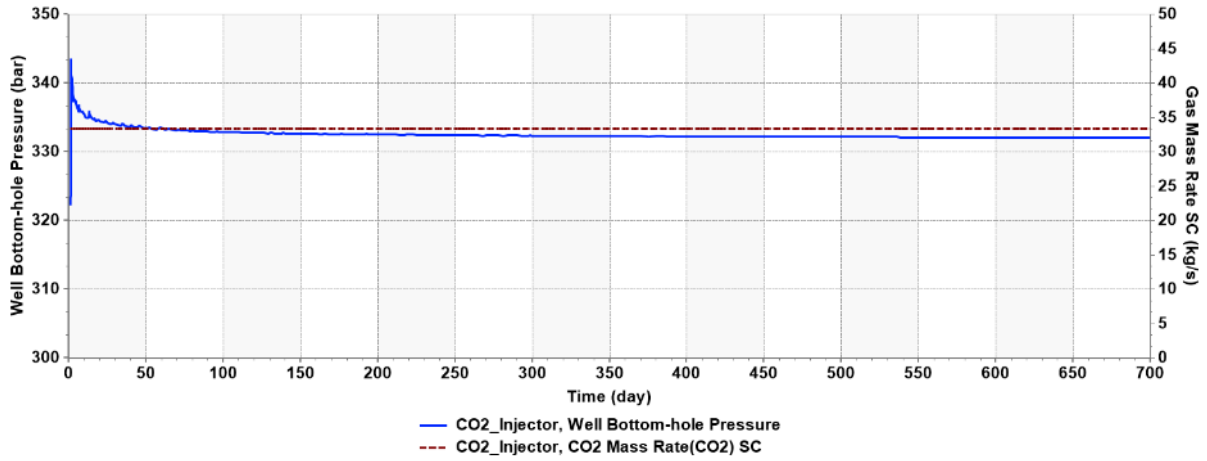

Figure 17: Simulated well bottomhole pressures and mass rates in the geothermal reservoir during plume setup period.

Figure 18 illustrates gas saturation profiles in the geothermal reservoir between the location of the injector well towards model boundaries at two depths representing potential perforation top (3000 m) and bottom (3070 m) for the producer at different injection time, 0.5-year, 1 year, 1.5 years as well as 2 years. Based on Ezekiel et al. 2022 study, it can be assumed that the minimum gas saturation that allows minimizing water production from the reservoir should be 0.4 in the cells near producer. Thus, the minimum gas saturation in the entire 70-m-long production interval, i.e., between the two depths of interest, must be 0.4. According to the figure, after 0.5 year of constant-rate injection, the condition is satisfied at a maximum distance of 75 m. With the onset of injection, this maximum distance can be extended up to 350 m if it lasts for 2 years.

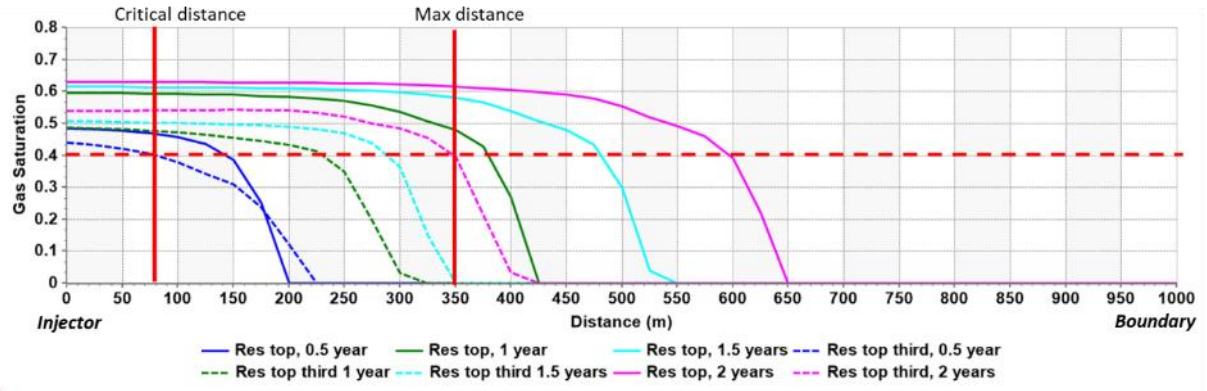

Figure 18: Gas saturation profiles in the geothermal reservoir around the injector well towards model boundaries at two depths representing perforation top and bottom for the producer (solid – reservoir top, dashed – bottomhole) for various plume setup durations: 0.5 year (blue), 1 year (green), 1.5 years (cyan) and 2 years (pink). The dashed line represents the desired minimum gas saturation at producer bottomhole.

We define thermal breakthrough as temperature drop by 1% from initial value. Figure 19 shows temperature profiles in the geothermal reservoir between the location of the injector well towards model boundaries at two depths representing potential perforation top (3000 m) and bottom (3070 m) for the producer at different injection time, 0.5-year, 1 year, 1.5 years as well as 2 years. According to the figure, thermal breakthrough can be satisfied if the well spacing has a critical distance of 40 m in case of 2-year-long plume configuration period.

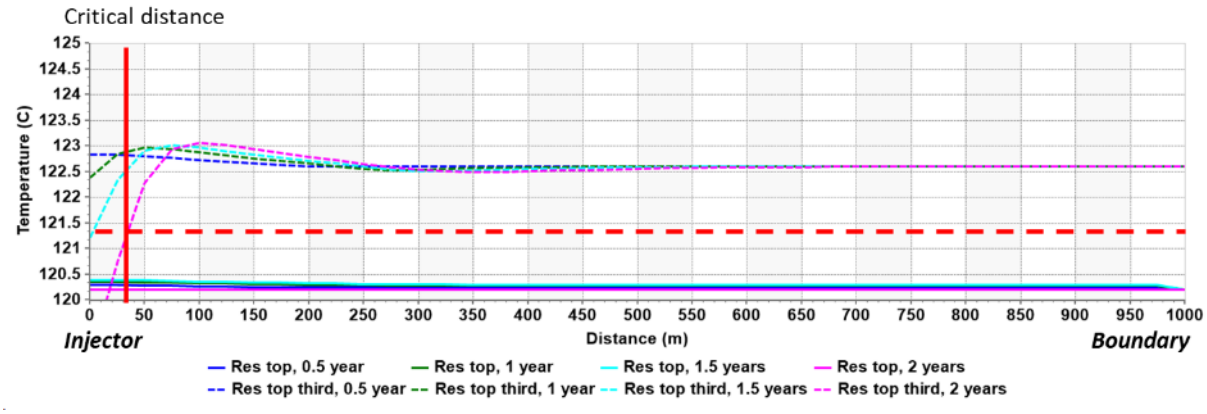

Figure 19: Temperature profiles in the geothermal reservoir around the injector well towards model boundaries at two depths representing perforation top and bottom for the producer (solid – reservoir top, dashed – bottomhole) for various plume setup durations: 0.5 year (blue), 1 year (green), 1.5 years (cyan) and 2 years (pink). The dashed line represents the desired minimum gas saturation at producer bottomhole.

Considering gas saturation and thermal criteria as well as potential variation of optimal well spacing due to sensitivity of the geological parameters, thus we choose a well spacing of 120 m for the cyclic injection and production cycles.

The results for the simulation of charge/discharge cycles and the sensitivity analysis can be found in Appendix 3, part D.

3.5 SALT CAVITIES SCENARIO

In the salt cavities scenario, there is a single well connected to each cavity, so that it works as injector during the charge phase and as back-producer during the discharge phase. The preliminary analysis of the system is performed according to the high efficiency CO_2 transcritical cycles following on the analysis developed in deliverable D3.1. The main thermodynamic properties of the charge and discharge cycles are given in the Table 8.

Table 8: Thermodynamic properties of charge and discharge cycles for the salt cavity scenarios.

Ref	Pressure (bar)	Temp (ºC)	Quality	Specific enthalpy (kJ/kg)	Specific entropy (kJ/kg K)	Density (kg/m3)
1	31.3	-4	1	432.95	1.87	86.02
2	200	153.2	-1	528.4	1.89	321.21
3	200	26.2	-1	246.88	1.1	908.63
4	31.3	-4	0.16	229.2	1.11	364.49
5	38.69	4	0	209.95	1.03	902.55
6	200	18.2	-1	230.15	1.04	945.04
7	200	121.7	-1	472.71	1.76	395.76
8	38.69	4	0.94	415.15	1.78	117.15

For the analysis of CO_2 injection during the charging phase, considering salt cavities as a geological reservoir, the Table 9 summarizes the assumptions that have been considered in the salt cavity injection calculations.

Table 9: Single cavity test cases.

Depth (m)	500	1000	1500
Maximum Pressure (MPa)	8.63	17.27	25.9
Minimum Pressure (Mpa)	3.23	6.48	9.71
Initial cavity pressure (MPa)	33	66	99
Initial cavity temperature (ºC)	30	45	60
Wellhead Injection pressure (MPa)	2.99	5.14	6.3
Wellhead Injection Temperature (ºC)	-5.6	12.2	14
Mass flow rate (kg/s)	100		
Well diameter (cm)	50		
Cycle duration (h)	5		

The CO_2 pressure is considered to be close to the lower limit, which is set according to the lithostatic pressure. The injection temperature is the temperature that the CO_2 acquires after expanding from the outlet of the high temperature exchanger. Figure 20 shows a P-h diagram for each of the cases considered in the study.

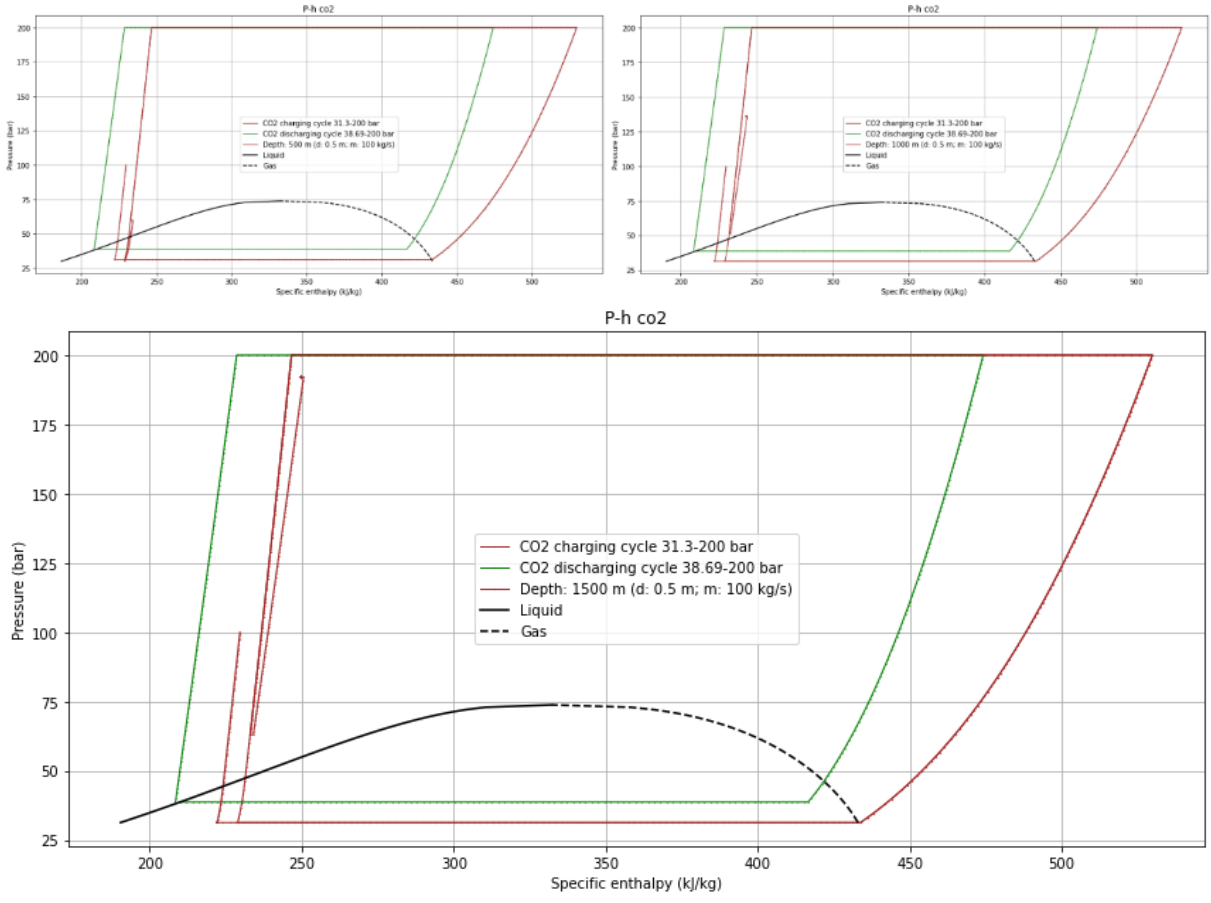

Figure 20: Pressure-enthalpy diagrams for the tested cases.

The pressure increase is considerable inside the pipe, especially in the 1000 and 1500 m cases. Table 10 shows a summary of the main thermodynamic properties as a function of depth.

Table 10: Thermodynamic properties as a function of depth.

	P (bar)	Temp (ºC)	Quality	P (bar)	Temp (ºC)	Quality	P (bar)	Temp (ºC)	Quality
Depth		500			1000			1500	
Plume	33	30		66	45		99	60	
Transport	100	15	-1	100	15	-1	100	15	-1
1	31.3	-4	0.13	31.3	-4	0.13	31.3	-4	0.13
2	31.3	-4	1	31.3	-4	1	31.3	-4	1
3	200	153.2	-1	200	153.2	-1	200	153.2	-1
4	200	26.2	-1	200	26.2	-1	200	26.2	-1
Wellhead	29.92	-5.6	0.17	51.4	12.6	-1	63	14	-1
Bottomhole	59.82	13.9	-1	136.27	21.9	-1	192.09	27.2	-1

A more detailed analysis of the CO_2 evolution inside the pipe during the injection phase is shown below. For each case analysed, a grouping of four graphs is shown, corresponding to pressure (bar), temperature (ºC), density (kg/m3) and velocity (m/s) as a function of the depth reached.

In the first of the cases analysed (500 m depth), the differentiation of two zones can be clearly observed (Figure 21). This is due to the fact that in this case, there is a slight change of state in the CO_2, according to the conditions imposed by the model.

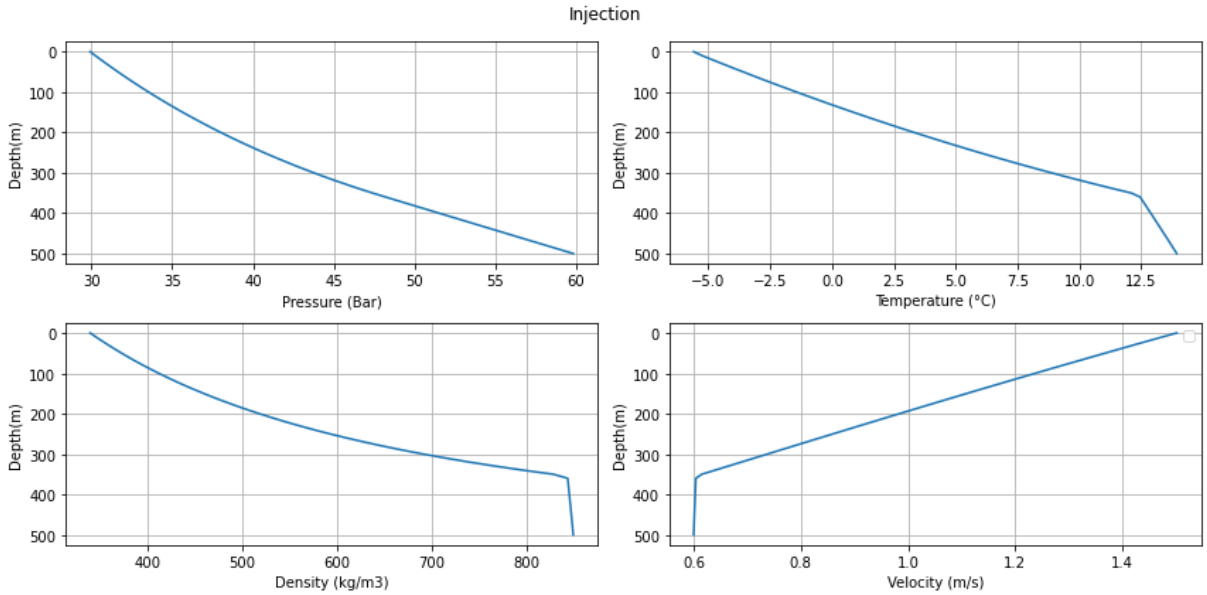

Figure 21: Injection into salt cavities (500 m).

For the 1000 and 1500 m cases (Figure 22 and Figure 23), the evolution of all parameters is fairly linear. It is worth mentioning a pronounced increase in pressure, which can lead to very high values in the bottomhole, although at all times they are within the limits established according to the lithostatic

pressure. The velocity is below 0.6 m/s. It is possible that for these conditions of mass flow (100 kg/s), a smaller pipe diameter may be more suitable.

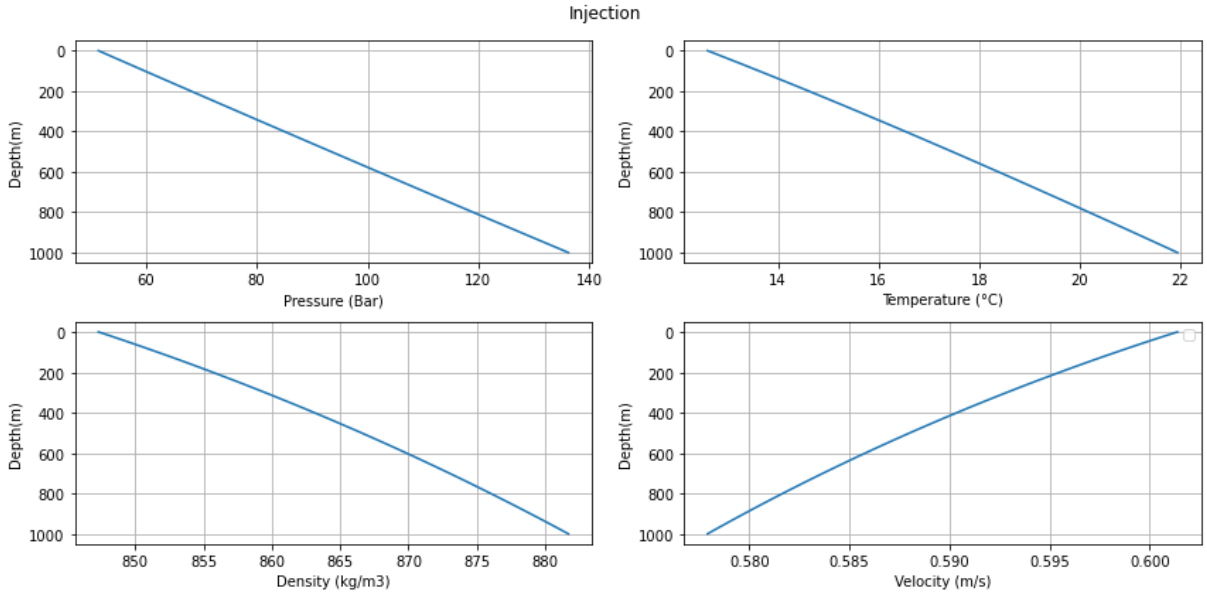

Figure 22: Injection into salt cavities (1000 m).

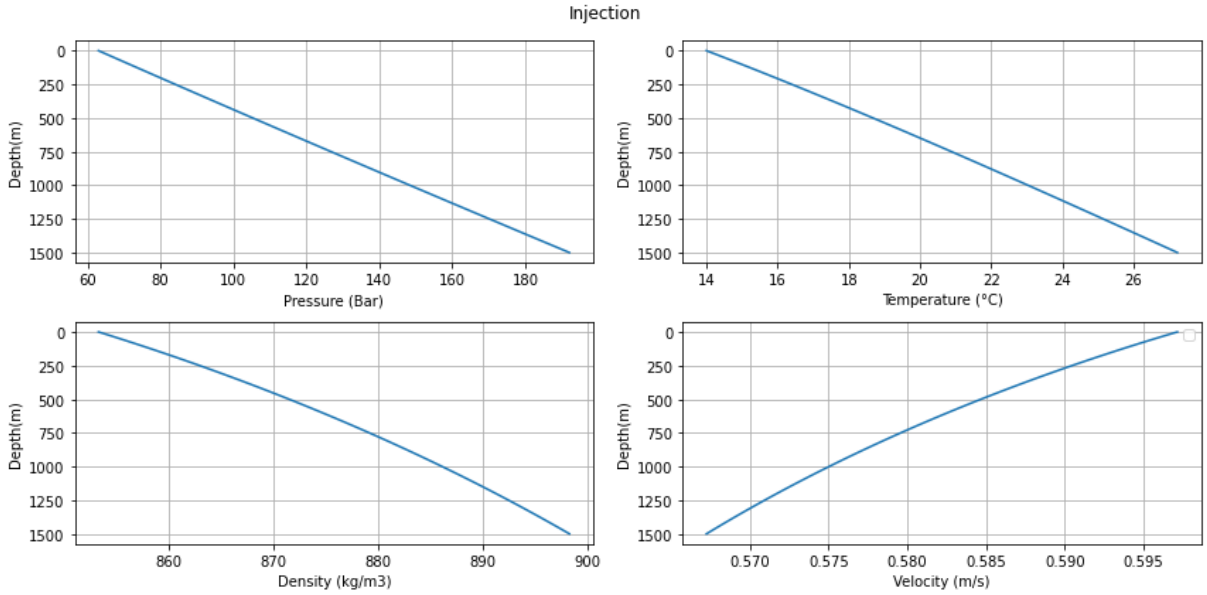

Figure 23: Injection into salt cavities (1500 m).

The technical analysis of the system shows a round-trip efficiency in the range of 47.2-55.2 %, with 5.52 hours of discharge available in the hot water thermal storage tank and 4.72 hours in the ice storage tank, for every 10 hours of charging (considering the same net power in the charging and discharging cycles, and closed loop operation).

4 CONCLUSIONS AND RECOMMENDATIONS

The analysis of the transient behaviour of the CO_2 in the geological reservoirs and wellbores is essential to understand the efficiency of the subsurface component of the CEEGS concept and the sustainability of the energy storage system. This was tested for several real-world scenarios in porous media reservoirs, involving deep saline aquifers and geothermal reservoirs. Several variants and configurations were considered for the deep saline aquifer scenarios, including open-boundaries and closed-boundaries aquifers, the influence of heterogeneity and anisotropy, and utilization of a single aquifer for injection and back-production of CO_2 or the utilization of two aquifers at different depths.

The analysis was based on numerical simulations of the subsurface component of CEEGS in geological conditions being considered for CO_2 storage in Portugal and Spain and for geothermal development in Germany. The selection of these real-world cases ensured that the scenarios were considering realistic conditions, but were supplemented by extensive sensitivity analysis, to find the parameters that will impact most significantly the feasibility and efficiency of CEEGS.

It is demonstrated that the feasibility of the CEEGS concept is lower for shallow aquifer depths, with the scenario with top reservoir depth at 850 m depth resulting in the lowest gross efficiencies. The same conclusion was derived from the two-aquifer scenario, in which the shallower aquifer, allowing for storage of CO_2 in gaseous state proved ineffective and not worth pursuing in further studies. A further issue favouring higher depth reservoirs is the decreasing proportion of produced brine with the increasing reservoir depth.

The closed boundaries deep saline aquifer raised concerns about the amount of brine produced with the CO_2, with the amount of produced brine increasing along the six cycles tested, although always remaining a low proportion of the total flow rate. Furthermore, the closed boundaries situation implies (as expected) lower mass flow rates due to the pressure buildup constrains.

The open boundaries DSA scenario, with considerable reservoir depth, and the geothermal scenario retrieved the most interesting gross efficiencies and sustainability, as measured by the well injectivities and well productivities. This reflects the importance of the reservoir temperature to the efficiency of the system, since higher depths, even high normal geothermal gradients, allow to obtain higher wellhead temperatures during the discharge phase.

The scenarios in which the geological reservoir is a salt cavity were studied with a semi-analytical approach integrating in MATLAB and Python the subsurface components (wellbores and salt cavity) with the surface facilities, to obtain the roundtrip efficiency of the CEEGS technology (and not only for the subsurface components as in the porous media reservoirs). In the scenarios tested, for three different cavity depths (500m, 1000m and 1500m). the efficiency varied from 47.2% to 55.2 %.

Some major concerns need to be addressed in subsequent tasks. It is necessary to understand the effects of the chemical composition of fluid at the producing wellhead, due to chemical reactions between CO_2-rock-brine in the reservoir. Also, the challenges imposed by the intermittency of injection and production of CO_2 need to be carefully considered. This can partly be solved by a strategy in which one the wells is continuously injecting CO_2 produced from a stationary source (charge phase) or from a mixture of CO_2 from the stationary source and CO_2 produced by the second well (discharge phase). This strategy would maximise the amount of permanently sequestered CO_2, but the intermittency would still exist in the production well.

The scenarios testing for reservoir heterogeneity and anisotropy in permeability also raised some concern about the degree of CO_2 saturation that can be attained around the production wells. Modelling of the Ketzin and Hontomin cases, to be conducted in WP4 should pay particular attention to those issues.

References

Adams, B. M., Kuehn, T. H., Bielicki, J. M., Randolph, J. B., and Saar, M. O., 2014, On the importance of the thermosiphon effect in CPG (CO_2 plume geothermal) power systems: Energy, v. 69, 409-418.

Allen, R.D., Doherty, T.J., Thoms, R.L., 1982. Geotechnical factors and guidelines for storage of compressed air in solution-mined salt cavities. Pacific Northwest Lab., Richland, WA (USA).

Bell, I. H., Wronski, J., Quoilin, S., and Lemort, V., 2014, Pure and Pseudo-pure Fluid Thermophysical Property Evaluation and the Open-Source Thermophysical Property Library CoolProp: Industrial & Engineering Chemistry Research, v. 53, no. 6, 2498-2508.

Bennion, B., and Bachu, S., 2005, Relative Permeability Characteristics for Supercritical CO_2 Displacing Water in a Variety of Potential Sequestration Zones in the Western Canada Sedimentary Basin: Proceedings of the 2005 SPE Annual Technical Conference and Exhibition held in Dallas, Texas, U.S.A., 9 – 12 October 2005, SPE 95547.

Bennion, B., and Bachu, S., 2006, The Impact of Interfacial Tension and Pore-Size Distribution/Capillary Pressure Character on CO_2 Relative Permeability at Reservoir Conditions in CO_2-Brine Systems: Proceedings of the 2006 SPE/DOE Symposium on Improved Oil Recovery held in Tulsa, Oklahoma, U.S.A., 22–26 April 2006, SPE 99325.

Cacace, M., Blöcher, G., Watanabe, N., Moeck, I., Bürsing, N., Scheck-Wenderoth, M., Kolditz, O., and Huenges, E., 2013, Modelling of fractured carbonate reservoirs: outline of a novel technique via a case study from the Molasse Basin, southern Bavaria, Germany: Environmental Earth Sciences, vol. 70, 3585-3602.

CMG - Computer Modelling Group Ltd, 2023, GEM Compositional & Unconventional Simulator, CMOST Intelligent Optimization & Analysis Tool and STARS Thermal & Advanced Processes Simulator, Available at: https://www.cmgl.ca.

Ezekiel, J., Ebigbo, A., Adams, B. M., and Saar, M. O., 2020, Combining natural gas recovery and CO_2-based geothermal energy extraction for electric power generation: Applied Energy, vol. 269, 115012.

Ezekiel, J., Adams, B., M., Saar, M. O. and Ebigbo, A., 2022, Numerical analysis and optimization of the performance of CO_2-Plume Geothermal (CPG) production wells and implications for electric power generation: Geothermics, vol. 98, 102270.

Fleming, M. R., Adams, B. M., Ogland-Hand, J. D., Bielicki, J. M., Kuehn, T. H., and Saar, M. O., 2022, Flexible CO_2-plume geothermal (CPG-F): Using geologically stored CO_2 to provide dispatchable power and energy storage: Energy Conversion and Management, vol. 253, 115082.

Haaland S.E. , 1983, Simple and explicit formulas for the friction factor in turbulent pipe flow. Journal of Fluids Engineering 1983;105:89-90.

Horváth, F., Musitz, B., Balázs, A., Végh, A., Uhrin, A., Nádor, A., Koroknai, B., Pap, N., Tóth, T., and Wórum, G., 2015, Evolution of the Pannonian basin and its geothermal resources: Geothermics, vol. 53, 328-352.

Huenges, E. (ed.), 2010, Geothermal Energy Systems: Exploration, Development, and Utilization: Wiley-VCH Verlag, Weinheim, Germany.

Kempka, T., Kühn, M., Class, H., Frykman, P., Kopp, A., Nielsen, C. M. and Probst, P., 2010, Modelling of CO_2 arrival time at Ketzin – Part I: International Journal of Greenhouse Gas Control, vol. 4, 1007-1015.

Khaledi, K., Mahmoudi, E., Datcheva, M., Schanz, T., 2016. Analysis of compressed air storage caverns in rock salt considering thermo-mechanical cyclic loading. Environ. Earth Sci. 75, 1–17. https://doi.org/10.1007/s12665-016-5970-1

Knapek, E., and Kittl, G., 2007, Unterhaching Power Plant and Overall System: Proceedings of the European Geothermal Congress 2007, Unterhaching, Germany, 30 May - 1 June 2007.

Koroncz, P., Vizhányó, Z., Farkas, M. P., Kuncz, M., Ács, P., Kocsis, G., Mucsi, P., Fedorné Szász, A., Fedor, F., and Kovács, J., 2022, Experimental Rock Characterisation of Upper Pannonian Sandstones from Szentes Geothermal Field, Hungary: Energies, vol. 15, 9136.

Lenkey, L., Mihályka, J., and Paróczi, P., 2021, Review of geothermal conditions of Hungary: Földtami Közlöny, vol. 151, no. 1, 65-78.

Liu, H., He, Q., Borgia, A., Pan, L., and Oldenburg, C. M., 2016, Thermodynamic analysis of a compressed carbon dioxide energy storage system using two saline aquifers at different depths as storage reservoirs: Energy Conversion and Management, vol. 127, 149-159.

Moeck, I. S., 2014, Catalog of geothermal play types based on geologic controls: Renewable and Sustainable Energy Reviews, vol. 37, 867-882.

Moeck, I. S., Dussel, M., Weber, J., Schintgen, T., and Wolfgramm, M., 2020, Geothermal play typing in Germany, case study Molasse Basin: a modern concept to categorise geothermal resources related to crustal permeability: Netherlands Journal of Geosciences, vol. 98, no. e14.

Ogland-Hand, J., D., Bielicki, J. M., Adams, B. M., Nelson, E. S., Buscheck, T. A., Saar, M. O., and Sioshansi, R., 2021, The value of CO_2-Bulk energy storage with wind in transmission-constrained electric power systems: Energy Conversion and Management, vol. 228, 113548.

Okoroafor, E. R., Saltzer, S. D., and Kovscek, A. R., 2022, Toward underground hydrogen storage in porous media: Reservoir engineering insights: International Journal of Hydrogen Energy, vol. 47, 33781-33802.

Oldenburg, C. M., and Pan, L., 2013, Porous Media Compressed-Air Energy Storage (PM-CAES): Theory and Simulation of the Coupled Wellbore–Reservoir System: Transport in Porous Media, vol. 97, 201-221.

Rühaak, W., Heldmann, C.-D., Pei, L., and Sass, I., 2017, Thermo-hydro-mechanical-chemical coupled modeling of a geothermally used fractured limestone: International Journal of Rock Mechanics and Mining Sciences, vol. 100, 40-47.

Soubeyran, A., Rouabhi, A., and Coquelet, C., 2019, Thermodynamic analysis of carbon dioxide storage in salt caverns to improve the Power-to-Gas process: Applied Energy, v. 242, p. 1090-1107.

Tóth, A. N., Szűcs, P., Pap, J., Nyikos, A., and Fenerty, D. K., 2018, Converting Abandoned Hungarian Oil and Gas wells into Geothermal Sources: Proceedings of the 43rd Workshop on Geothermal Reservoir Engineering Stanford University, Stanford, California, February 12-14, 2018, SGP-TR-213.

Varga, A., Bozsó, G., Garaguly, I., Raucsik, B., Bencsik, A., and Kóbor, B., 2019, Cements, Waters, and Scales: An Integrated Study of the Szeged Geothermal Systems (SE Hungary) to Characterize Natural Environmental Conditions of the Thermal Aquifer: Geofluids, vol 2019, 4863814.

Willems, C. J. L., Cheng, C., Watson, S. M., Minto, J., Williams, A., Walls, D., Milsch, H., Burnside, N. M., and Westaway, R., 2021, Permeability and Mineralogy of the Újfalu Formation, Hungary, from Production Tests and Experimental Rock Characterization: Implications for Geothermal Heat Projects: Energies, vol. 14, 4332.

Wilkinson, M. (editor) 2023. Deliverable 2.7 – Conceptual Geological Models of the Portugal, Spain and France. PilotSTRATEGY project, Grant Agreement: 101022664.

Wolfgramm, M., Bartels, J., Hoffmann, F., Kittl, G., Lenz, G., Seibt, P., Schulz, R., Thomas, R., and Unger, H. J., 2007, Unterhaching geothermal well doublet: structural and hydrodynamic reservoir characteristic; Bavaria (Germany): Proceedings of the European Geothermal Congress 2007, Unterhaching, Germany, 30 May - 1 June 2007.